U.S.N.A. ---Trident Scholar project report; no. 316 (2003)

Design Specifications Development for Unmanned Aircraft Carrier Landings: A Simulation Approach

by

Midshipman Joseph F. Sweger, Class of 2003
United States Naval Academy
Annapolis, Maryland

_____
(signature)

Certification of Advisers Approval

CAPT Robert Niewoehner USN
Department of Aerospace Engineering

_____
(signature)

_____
(date)

Acceptance for the Trident Scholar Committee

Professor Joyce E. Shade
Deputy Director of Research & Scholarship

_____
(signature)

_____
(date)

Report Documentation Page

Form Approved
OMB No. 0704-0188

Public reporting burden for the collection of information is estimated to average 1 hour per response, including the time for reviewing instructions, searching existing data sources, gathering and maintaining the data needed, and completing and reviewing the collection of information. Send comments regarding this burden estimate or any other aspect of this collection of information, including suggestions for reducing this burden, to Washington Headquarters Services, Directorate for Information Operations and Reports, 1215 Jefferson Davis Highway, Suite 1204, Arlington VA 22202-4302. Respondents should be aware that notwithstanding any other provision of law, no person shall be subject to a penalty for failing to comply with a collection of information if it does not display a currently valid OMB control number.

1. REPORT DATE	2. REPORT TYPE	3. DATES COVERED
02 MAY 2003	**N/A**	**-**

4. TITLE AND SUBTITLE	5a. CONTRACT NUMBER
Design Specifications Development for Unmanned Aircraft Carrier Landings: A Simulation Approach	5b. GRANT NUMBER
	5c. PROGRAM ELEMENT NUMBER
6. AUTHOR(S)	5d. PROJECT NUMBER
	5e. TASK NUMBER
	5f. WORK UNIT NUMBER
7. PERFORMING ORGANIZATION NAME(S) AND ADDRESS(ES) **United States Naval Academy Annapolis, Maryland 21402**	8. PERFORMING ORGANIZATION REPORT NUMBER
9. SPONSORING/MONITORING AGENCY NAME(S) AND ADDRESS(ES)	10. SPONSOR/MONITOR'S ACRONYM(S)
	11. SPONSOR/MONITOR'S REPORT NUMBER(S)

12. DISTRIBUTION/AVAILABILITY STATEMENT
Approved for public release, distribution unlimited

13. SUPPLEMENTARY NOTES
The original document contains color images.

14. ABSTRACT

15. SUBJECT TERMS

16. SECURITY CLASSIFICATION OF:			17. LIMITATION OF ABSTRACT	18. NUMBER OF PAGES	19a. NAME OF RESPONSIBLE PERSON
a. REPORT	b. ABSTRACT	c. THIS PAGE			
unclassified	**unclassified**	**unclassified**	**UU**	**72**	

Standard Form 298 (Rev. 8-98)
Prescribed by ANSI Std Z39-18

ABSTRACT

This project investigated the demands landing precision place upon the physical configurations of carrier-based unmanned aircraft. The goal was the determination of a minimum set of performance and maneuverability criteria that ensure satisfactory carrier landing precision and consistency. The first step was to design and write a comprehensive computer model to simulate unmanned carrier landings. The model included ship dynamics, atmospheric turbulence, navigational inaccuracies, dynamic airplane control structure, and aircraft dynamics. The airplane sensed and corrected for three disturbances: wind gusts, unsteady ship motion, and navigational information errors. The second step involved varying aircraft attributes and recording landing performance statistics for each configuration. The influence of each attribute was extracted from the landing statistics. This was done for various weather conditions because the ship motion increases with wave size and the gust intensity increases with average wind velocity. The third step was the development of preliminary design criteria to be refined and verified with test cases. The fourth and final step was to generate the final aircraft design limits. The longitudinal design limit is a lift curve slope of at least 2.9 per radian. No bound on instability or drag was indicated.

Keywords: UAV, UCAV, Automated Landing, Carrier-based

ACKNOWLEDGMENTS

First, I would like to thank my advisor, CAPT Niewoehner, for his constant help and guidance. I certainly could not have done this without him. I would like to thank the JPALS team at Patuxent River. They were kind enough to share test data for a JPALS error model. Eric Schug was very helpful. He showed me how to use the data and helped me with all the necessary coordinate transforms and conversions. Professor Pierce was invaluable in helping to analyze the Fourier transform of the error signal. He also introduced and showed me how to use additional tools to look at the time variant frequency content of the signal. LCDR Hallberg also played a vital role, devising a successful control structure after this project had suffered months of dead ends. The Trident Committee members provided guidance and gave me this incredible opportunity. I would also like to thank all of my instructors who have prepared me for this over the last several years. I could not have done any of this alone.

Preface

Unmanned systems are becoming increasingly important to our military. The Chief of Naval Operations (CNO), Admiral Clark, has stated that advancing technology will have a vital role in the future of the navy in "Sea Power 21"[1]. Recent operations in Afghanistan and Iraq showed that this means unmanned systems, particularly unmanned air vehicles (UAV).

Automated landings are not new. The Automatic Carrier Landing System (ACLS) has been in use for years, but it was not flight critical because the pilot provided for reversion to manual control. Consequently, airplanes had been designed for good piloted handling qualities; if he could handle the airplane, the automatic control system had no difficulty doing the same. Going to a fully autonomous system permits greater design freedom, no longer constrained by the limitations of the human operator. The question is how much? This research is intended to begin to answer that question by defining the design constraints imposed by fully autonomous carrier landings. This then is a prerequisite technology to the implementation of the CNO's vision.

[1] Clark, V. "Sea Power 21".

Table of Contents

ABSTRACT 1
ACKNOWLEDGMENTS 2
BACKGROUND 8
MANNED VS UNMANNED 11
PROBLEM STATEMENT 11
METHOD OF INVESTIGATION 12
FIGURES OF MERIT 12
MODEL INTRODUCTION 13
SIMULATION NOISE SOURCES 15
SHIP DYNAMICS 15
JPALS NAVIGATION ERRORS 20
DRYDEN GUST 21
AIRCRAFT DYNAMICS 23
CONTROL STRUCTURE 24
LANDING SIMULATIONS 30
RESULTS AND DISCUSSION 33
SINGLE SIMULATION RUNS 33
DISTURBANCE SOURCES 37
INFLUENCE OF LIFT CURVE SLOPE AND LONGITUDINAL STABILITY 39
INFLUENCE OF LIFT CURVE SLOPE AND DRAG COEFFICIENT 50
SUMMARY AND DESIGN IMPLICATIONS 52
CONCLUSIONS 54
RECOMMENDATIONS 55
BIBLIOGRAPHY 55
APPENDIX I : LONGITUDINAL SIMULATION CODE (version 20.03.03) 57
APPENDIX II : PLAN OF ACTION AND MILESTONES 63
APPENDIX III : SHIP MOTION SIMULATION CODE 66

Table of Figures

Figure 1 : Carrier Landing Environment 10
Table 1: Touchdown Dispersion Parameters 10
Figure 2: Model Architecture 14
Table 2 : RMS Amplitudes for Modeled Sea-states 17
Figure 3: Ship States in Sea-State 3 18
Figure 4: Resulting Landing Area Displacement Due to Ship Motion 19
Table 3: Maximum Vertical Landing Area Displacement Due to Ship Motion 19
Table 4 : Standard Deviation of JPALS Errors 21
Figure 5: JPALS Vertical Navigational Error 21
Figure 6: Model Generated Gust Field 23
Figure 7: Aircraft Sign Conventions and Notation 24
Figure 8: Implementation Model for State Feedback Controller using Kaminer's Delta Method 26
Figure 9: Graphical Depiction of Control Structure Implementation 27
Table 5: All Simulated Test Conditions 32
Figure 10: Preliminary Single Simulation Flight Path and Error 34
Figure 11: Flight Path History at Sea-state 5 36
Figure 12: Disturbances' Influence on Aircraft States 36
Figure 13: Landing Position Error Statistics for Each Noise Component 38
Table 6: Combination Effects of Disturbance Sources 39
Figure 14: Sea-state 4 Boarding Rate Contour 40
Figure 15: Sea-state 5 Boarding Rate Contour 41
Figure 16: Sea-state 5 Landing Position Error Standard Deviation Contour 42
Figure 17: Sample Landing Error Distribution for Sea-state 5 43
Figure 18: Sea-state 5 Pitch Angle Standard Deviation Contour 45
Figure 19: Sea-state 5 RMS Elevator Control Power 46
Figure 20: Sea-state 4 RMS Elevator Control Power 47
Figure 21: Sea-state 5 RMS Throttle Control Power 48
Figure 22: Sample Sea-state 5 Control Histories 49
Figure 23: Sea-state 3 Landing Position Error Standard Deviation Contour 51
Figure 24: RMS Throttle Control Power for Sea-state 3 52

List of Symbols

C_{Do}	Drag coefficient at trim
C_L	Lift coefficient
$C_{l\alpha}$	Lift curve slope
C_m	Pitching moment coefficient
C_{m_α}	Pitching moment coefficient per unit AOA
g	Gravity
q	Pitch rate
u	Velocity component in X direction
u_0	Trim velocity
w	Velocity component in Z direction
α	Angle-of-attack of aircraft (AOA)
u/s	Integral of velocity perturbation in X direction
h	Altitude
h/s	Integral of altitude error
θ	Pitch attitude (angle)
ϕ	Roll or Bank angle
ψ	Yaw angle
$\bar{x}$	Vector of states (a bar over a variable indicates a vector quantity)
$\dot{\bar{x}}$	Time derivative of $\bar{x}$ (a dot over a variable indicates a time derivative)
Δ	Indicates that the following quantity is a perturbation value
$\bar{\eta}$	Vector of control inputs
δ	Elevator deflection angle
δ_T	Throttle position
$\bar{y}$	Vector of output variables
A	Matrix of aircraft dynamics coefficients
B	Matrix of control influences on aircraft dynamics
C	Matrix of coefficients relating aircraft states to output states
D	Matrix of coefficients relating control states to output states
J	Value of cost function
M	Pitching moment coefficient
Q	Matrix of cost factors for perturbations in aircraft states
R	Matrix of cost factors for control inputs
X	Aerodynamic force in x direction
Y	Aerodynamic force in y direction
Z	Aerodynamic force in z direction
X_u	$\frac{\partial X}{\partial u}$ (Change in X per unit change in u)
X_w	$\frac{\partial X}{\partial w}$ (Change in X per unit change in w)
Z_u	$\frac{\partial Z}{\partial u}$ (Change in Z per unit change in u)

Z_w	$\frac{\partial Z}{\partial w}$	(Change in Z per unit change in w)
M_u	$\frac{\partial M}{\partial u}$	(Change in M per unit change in u)
M_w	$\frac{\partial M}{\partial w}$	(Change in M per unit change in w)
M_q	$\frac{\partial M}{\partial q}$	(Change in M per unit change in q)
X_δ	$\frac{\partial X}{\partial \delta}$	(Change in X per unit change in elevator deflection)
Z_δ	$\frac{\partial Z}{\partial \delta}$	(Change in Z per unit change in elevator deflection)
M_δ	$\frac{\partial M}{\partial \delta}$	(Change in M per unit change in elevator deflection)
$X_{\delta T}$	$\frac{\partial X}{\partial \delta_T}$	(Change in X per unit change in throttle)
$Z_{\delta T}$	$\frac{\partial Z}{\partial \delta_T}$	(Change in Z per unit change in throttle)
$M_{\delta T}$	$\frac{\partial M}{\partial \delta_T}$	(Change in M per unit change in throttle)

BACKGROUND

Carrier landings define naval aviation. These landing requirements drive the design of both the aircraft and the ship, with the landing airspeed constituting one of the most significant attributes of the problem. The correct determination of the approach speed is vital. It is the balance of landing safely and causing unnecessary wear, which results in higher maintenance requirements and shorter service life. Higher landing speeds decrease the maximum landing weight. This means an aircraft must land with less ordnance and fuel. The determination of the approach speed for manned aircraft is the minimum speed that simultaneously satisfies several criteria. These criteria can be found in diverse military specifications and include the following[2]:

a. Aerodynamic stall margin of 10%
b. Field of view (over the nose visibility)
c. Flight qualities (defined in MIL-STD-8785/1797)
d. Compatibility with Wind Over the Deck (WOD)
e. Longitudinal Acceleration in level flight of 5 ft/sec^2 within 2.5 seconds in full power
f. Pop-up, 50 ft. glide slope transfer with stick only in 5 seconds
g. Minimum single engine rate of climb: 500 ft/min (tropical day)

The goal of landing speed criteria is to facilitate the design of aircraft that can consistently make safe carrier landings. These historic requirements were recently reviewed for manned aircraft. While Navy contractors have performed simulation trials of aircraft under design, no criteria exist for unmanned aircraft distinct from manned. No study has been done to determine

[2] Rudowski *et al*, Review of Carrier Approach Criteria for Carrier-based Aircraft p.22

the range of aircraft attributes necessary for an unmanned aircraft to land safely. The referenced Heffley report attempted to perform this evaluation for the case of manned aircraft[3].

Understanding the carrier-landing task requires some discussion of terminology. Angle of attack (AOA) is the angle between where the airplane is pointed and where it is going. This value along with the velocity determines the amount of lift generated. An aircraft's pitch angle is where the nose is pointed relative to the horizon and for manned aircraft strongly influences the over the nose visibility from the cockpit. Sink rate is the vertical component of the velocity. The glide slope is the desired airplane trajectory, terminating at the desired touch-down point, nominally a straight line extending 3.5 degrees above the horizon as shown in Figure 1 below.[4] Flight-path angle is the angle between the airplane's velocity vector and the horizon. Because the ship (and touchdown point) is typically moving through the water at 10 to 20 knots, maintaining a 3.5 degree glide slope relative to the ship results in a flight-path angle of 3.0 degrees relative to the inertial frame. The four wires highlighted in Figure 1 are called cross-deck pendants. The cross-deck pendants are disposable and are replaced after 100 hits or sooner if damaged. They are attached to the purchase cable, which goes into the arresting engine under the deck. The maximum energy absorption capability of this system constitutes one of the most significant constraints to the landing problem. Additionally, the targeted hook touch down point is labeled.

The ultimate objective of every carrier approach is a safe arrested landing, or trap. There are many constraints to the landing task. Structures and safety physically constrain carrier landings, while operational requirements demand a high boarding rate (the percentage of approaches that result in a trap). Off-centerline landings are dangerous due to the proximity of

[3] Heffley, *Outer-Loop Control Factors For Carrier Aircraft*.
[4] Waters, "Ship Landing Issues" PowerPoint.

personnel and equipment; short (low) approaches hazard striking the aft end of the ship. High approaches will fail to catch a wire. The structural limits of the hook and cross-deck pendant determine the maximum landing velocity. Sink rate is limited by the landing gear structure. Additionally, hook geometry requires the aircraft to land with a positive pitch angle, optimally five degrees, because the main gear must touchdown first. The positive pitch angle is also necessary for the hook to engage the wire. The target touchdown dispersions, developed from the desired boarding rates, are tabulated in feet in Table 1.[5] Both desired performance and the maximum allowable performance are given.

Figure 1 : Carrier Landing Environment[6]

Table 1: Touchdown Dispersion Parameters[7]

	Target Performance (ft	Maximum Allowable (ft)
Lateral Mean	2	4
Lateral Std Deviation	3	5
Longitudinal Mean	16	24
Longitudinal Std Deviation	40	60

[5] Waters, Test Results of an F/A-18 Automatic Carrier Landing Using Shipboard Relative GPS. p10.
[6] Waters, "Ship Landing Issues" PowerPoint.
[7] Waters, Test Results of an F/A-18 Automatic Carrier Landing Using Shipboard Relative GPS. p10.

MANNED VS UNMANNED

Historically, designing an airplane for the carrier-landing task has been constrained by the limitations of the pilot as an integral part of the control system. The full capabilities of automated control systems have never previously been explored. The human operator has difficulty tracking multiple parameters at once. Part of the difficulty is focusing one's vision on the ship for line-up and glide slope then back to instruments in the cockpit to read airspeed and angle of attack. People also lack the precision and reaction time of computers. Consequently, if an airplane's handling qualities satisfied a human pilot, the legacy automated systems (e.g. SPN-42 Automatic Carrier Landing System (ACLS)) could easily handle the airplane. Moreover, ACLS was neither flight critical nor attempted at severe sea-states. The move to unmanned systems permits design liberties fully capitalizing on the capabilities of an automated system, yet raises the automated system to the status of "flight critical". If the control system cannot successfully get the vehicle aboard, it is lost at sea.

PROBLEM STATEMENT

The above pre-requisite background now permits a concise statement of this study's aim. Given the disturbance environment characterized by realistic atmospheric turbulence, navigational inaccuracies, ship motion, the required performance metrics, and a specified controls strategy, define the major aerodynamic performance and controllability limitations upon the design of an autonomous carrier-based airplane. The problem is not, "given an airplane, find a control system that satisfies the performance requirements." Instead the goal is to define the

range of airplane attributes which, in concert with an automatic control system, can satisfy the Table 1 performance requirements.

METHOD OF INVESTIGATION

A Monte Carlo simulation approach was used. A sensitivity analysis of the influence of several characteristics of the airplane on the landing performance was conducted in the presence of representative disturbances, including navigation errors, gusts, and ship motion. These results were used to define the range of suitable airplane characteristics. This methodology is broken down into small pieces and given as a tabular timeline in Appendix II.

FIGURES OF MERIT

Operationally, boarding rate and safety are the primary concerns. From these, several other performance targets have been derived, such as landing dispersion and pitch attitude variation, which are easier for the engineers to use and tend to force designs to meet the operational needs. Landings from eighty feet short to sixty feet long would all achieve a successful arrestment, based solely on the placement of the four cross-deck pendants. This measurement, along with the desired boarding rate provided the origin of the landing dispersion requirements listed previously in Table 1.

The pitch attitude constraints come from several sources. The nose must be pitched up to avoid landing nose gear first and to reduce approach speed it is desirable to fly near stall speed. Excessive nose up pitch is unacceptable because of stall concerns and the hook is prone to skip over the wires. Large variations in pitch mean large variations in AOA as well. This is undesirable because it forces an increased stall margin and therefore an increased approach speed and lower allowable landing weight.

Finally, the total control power available from the control surfaces constitutes a major configuration feature of an airplane, particular at low speeds where the low dynamics pressure yields poor sensitivity (expressed in torque about the airplane center of gravity per degree of control deflection). For greater control power (which we'll express in root-mean-square (RMS) activity), faster or more powerful control actuators increase the weight and cost of those systems. This makes a high control power requirement undesirable.

MODEL INTRODUCTION

The simulation models consisted of multiple systems of differential equations. For example, the full six-degrees-of-freedom (6-DoF) aircraft dynamics model consists of twelve, first-order non-linear coupled differential equations. Due to time constraints, this study restricted itself to an investigation of the longitudinal behavior of the airplane (3-DoF). In this case, MATLAB was used to solve a discrete-time difference equation, numerically converted from six linear differential equations (two additional integrated states will appear later in the controller in order to provide integral action). Figure 2, the flow chart below, depicts a visualization of the unmanned carrier landing simulation system. The three sources of noise injected into the simulation are numbered circles. Although not shown here, each box contains another diagram depicting the interactions of the governing equations for that aspect of the system. The arrows show the flow of information from one sub-system to the next. Each simulation run terminated with the collection of a touchdown point and orientation. The MATLAB simulation code is attached as Appendix I. Comments are included in the code describing the function of parts of the code as well as limited explanations for what has been included and what has been neglected.

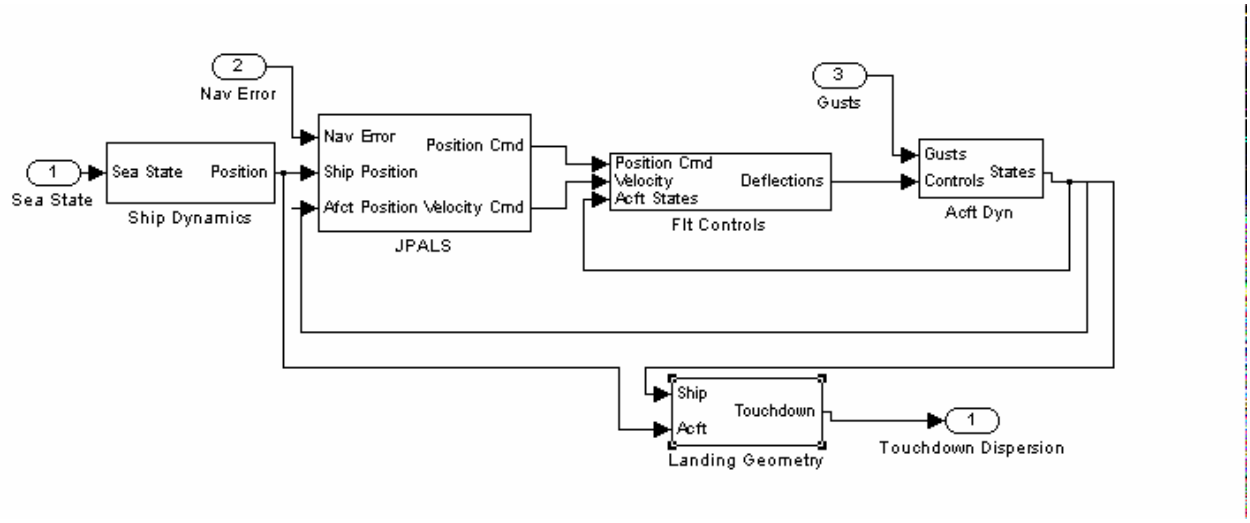

Figure 2: Model Architecture

The system was linearized for simulation. Landing approach can reasonably be treated as a linear perturbation problem about a trim state due to the size of the perturbations. Linear aerodynamics characterizes the approach problem; the lift curve slope may be assumed linear within the subject range of operation, below stall, as may the effectiveness of the control effectors. The small corrections keep the airplane below stall angle of attack. Therefore, the assumed linearity is valid.

The ordinary differential equations were solved by first linearizing the equations of motion and creating a state-space formulation of the form given below in equation 1.1 where: $\bar{x}$ is the vector of time-dependent aircraft states; $\dot{\bar{x}}$ is the time derivative of $\bar{x}$; $\bar{\eta}$ is the vector of control inputs; A is a matrix of time invariant constants whose values reflect the airplane's aerodynamic properties and whose eigenvalues describe the open-loop modes of the airplane; B is a matrix of time invariant constants whose values reflect the influence of the controls on the aircraft states; $\bar{y}$ is a vector of outputs; and C and D are matrices of constants that relate the aircraft states and control positions to the outputs specified in $\bar{y}$.

$$\begin{aligned} \dot{\bar{x}} &= A\bar{x} + B\bar{\eta} \\ \bar{y} &= C\bar{x} + D\bar{\eta} \end{aligned} \tag{1.1}$$

This type of system is described as linear time invariant, LTI, because the governing differential equations are linear and the coefficients are not time dependent. This continuous-time system was then converted by functions in the MATLAB Control Toolbox to a discrete time state-space formulation, which is solved numerically by constant-time-step difference equations of the form shown below where the subscripted '*d*' indicates a discrete time matrix.

$$\begin{aligned} \bar{x}(k+1) &= A_d \bar{x}(k) + B_d \bar{\eta}(k) \\ \bar{y}(k+1) &= C_d \bar{x}(k) + D_d \bar{\eta}(k) \end{aligned} \tag{1.2}$$

A ten-millisecond time step (0.01 sec) was selected to match the ship motion model (discussed below) provided by the Naval Air Systems Command (NAVAIR). This interval was more than fast enough to accurately model the aircraft dynamics linearly, with the sample rate over 100 times that of the fastest airplane dynamic mode. The time step was consequently much smaller than necessary, but the speed of the computational capability permitted this extravagance.

SIMULATION NOISE SOURCES

SHIP DYNAMICS

At the suggestion of engineers from NAVAIR, the dynamics and dimensions of CVN 65, the U.S.S. Enterprise, were employed throughout the study. The distances from the ship's center of motion to the landing area in feet are 223 aft, 64 up, and 10 left.

The ship dynamics model provided by NAVAIR generated six degree-of-freedom time histories of ship motion for a sea-state chosen by the user. The provided ship dynamics code is included in Appendix III. Ship pitch is positive nose up, roll is positive to the left, and yaw is positive nose left. Note that all ship displacements are referenced to the ship center of motion. Since the desired touch down point was displaced a significant vertical and horizontal distance from the center of motion, the touchdown point's translational displacement was dependent upon both the translational and angular displacements of the ship. These angles had to be converted to distances in X, Y, and Z to be useful to the landing task. Equations 1.3 through 1.5 given below are the exact relationships.

$$Z_{ch} = -223*\sin(S_{pitch}) + 64*\cos(S_{pitch})*\cos(S_{roll}) - 64 - 10*\sin(S_{roll}) \quad (1.3)$$

$$Y_{ch} = 64*\sin(S_{roll}) + 10*\cos(S_{pitch})*\cos(S_{yaw}) - 10 + 223*\sin(S_{yaw}) \quad (1.4)$$

$$X_{ch} = 223*\cos(S_{pitch})*\cos(S_{yaw}) - 223 + 64*\sin(S_{pitch}) - 10*\sin(S_{yaw}) \quad (1.5)$$

The system linearizes under a small angle assumption. At sea-state 5, the most severe conditions modeled, the RMS value for the ship's pitch was only 1.83 degrees, well within the small angle criterion. Under the small angle approximation, cosine terms go to unity and sine terms reduce to the angle expressed in radians. The resulting system is shown below as equations 1.6 through 1.8.

$$Z_{ch} = -223*S_{pitch} - 10*S_{roll} \quad (1.6)$$

$$Y_{ch} = 64*S_{roll} + 223S_{yaw} \quad (1.7)$$

$$X_{ch} = 64*S_{pitch} - 10*S_{yaw} \quad (1.8)$$

This system may be used to model the complete ship-aircraft system. Again, for the purposes of this report, only longitudinal dynamics were modeled. The effects of ship pitch alone are given in equations 1.9 and 1.10.

$$Z_{ch} = -223 * S_{pitch} \tag{1.9}$$

$$X_{ch} = 64 * S_{pitch} \tag{1.10}$$

"Surge", "heave", and "sway" describe linear translations of the ship about its center of motion fore or aft, up or down, and sideways respectively. These displacements were added directly to the translational displacement. Thus, the vertical and horizontal displacements of the landing area, due to the influence of ship motion are:

$$Z_{ch} = -223 * S_{pitch} + \text{heave} \tag{1.11}$$

$$X_{ch} = 64 * S_{pitch} + \text{surge} \tag{1.12}$$

For the purposes of this study, sea-states 3, 4, and 5 were modeled. Table 2 provides the relevant RMS amplitudes.

Table 2 : RMS Amplitudes for Modeled Sea-states

Sea-state	Heave (ft)	Surge (ft)	Pitch (deg)
3	2.11	0.838	0.763
4	3.81	1.4	1.22
5	5.06	2.1	1.83

Figure 3 below depicts the ship motion for sea-state 3. It is clear that the magnitudes and frequencies are different for each of the six ship states, due to both the incident wave angle, and the dramatically different moments of inertia. Because the frequencies for the ship motion were different, and the resulting movement of the landing area is a linear combination of those states,

a distinct "beating" pattern is observed. As the phase of the ship motion influenced the landing precision of the aircraft, care was taken to distribute the simulation initial conditions across the full spectrum of ship states. For the longitudinal problem, only half of these states have significant influence as shown in equations 1.11 and 1.12. The other three states are neglected for simplicity. The magnitudes in Figure 3 below show that the surge is less than half the magnitude of the heave. The surge must be scaled by the glide slope, or multiplied by 0.06, to arrive at the change in commanded altitude. Consequently, although surge is included in the model, its effect on the commanded altitude is only 3% of the influence of heave.

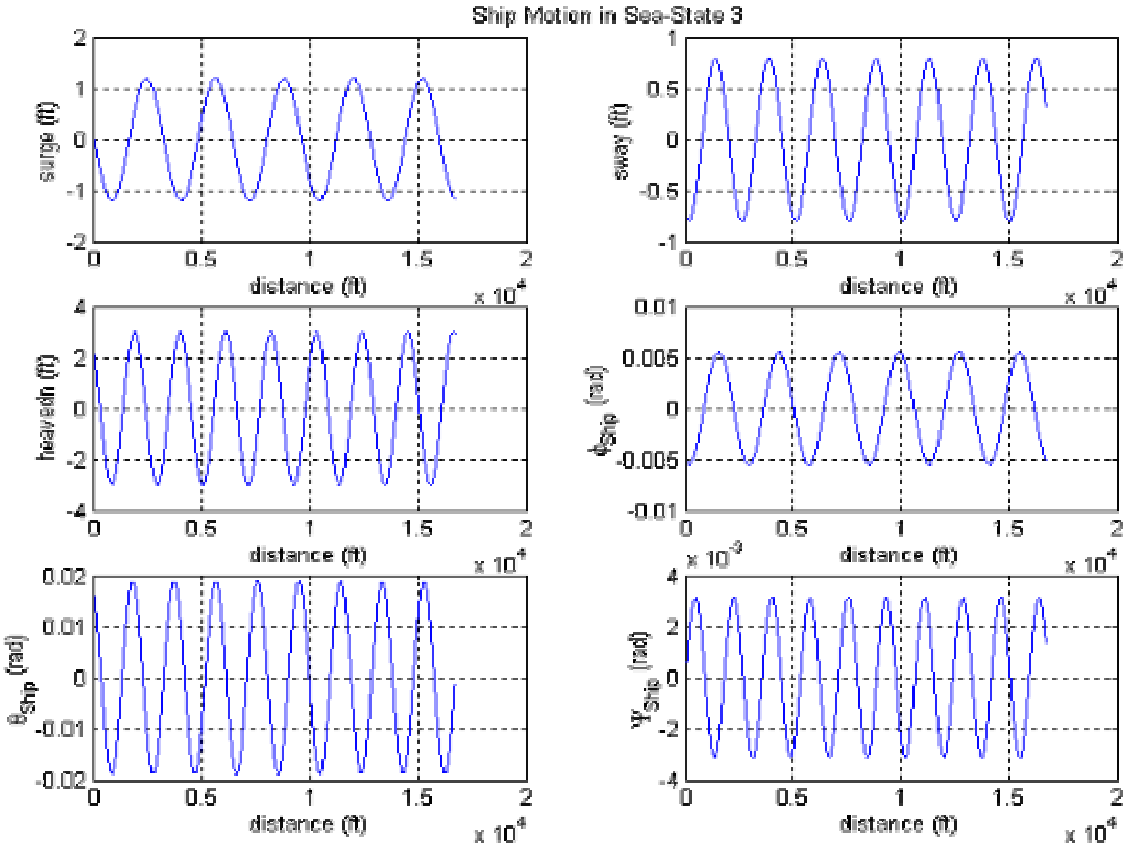

Figure 3: Ship States in Sea-State 3

For the longitudinal problem, pitch, heave, and surge influence the height of the target landing area about its mean position. The total influence of ship motion for all three modeled

sea-states is presented in Figure 4 below. The landing area vertical displacement is graphed in feet versus time. Local maximums occur approximately every 10 seconds for all three sea-states. Although the local maximums occur at nearly the same frequency for each sea-state, the frequency of the beats is more than twice as fast for sea-state 5 as for the other two, which are much closer. The absolute maximum displacements from Figure 4 are listed in Table 3 below.

Figure 4: Resulting Landing Area Displacement Due to Ship Motion

Table 3: Maximum Vertical Landing Area Displacement Due to Ship Motion

Sea-state	Max Vertical Displacement (ft)
3	7.1
4	12.0
5	17.2

JPALS NAVIGATION ERRORS

The Joint Precision Automated Landing System (JPALS), currently under development for use by both the Navy and Air Force, will surely serve as the guidance system on first generation unmanned shipboard aircraft. JPALS operates using differential-GPS data, blended with inertial navigation on both the airplane and the carrier. The blended data takes advantage of the high accuracy of inertial navigation systems over relatively short periods of time, updated by GPS at a lower frequency, in a process called complementary filtering. Differential GPS accuracy is achieved without correction factors because the critical value is the position of the aircraft relative to the ship as opposed to the absolute position of either in the world. The proximity of the ship and airplane during approach and landing cause both GPS receivers to experience the same atmospheric errors, resulting in very tight error bounds.

NAVAIR provided one and a half hours of JPALS flight test data sampled at 50 Hz. with both the measured and the true position. This data provided the basis for the navigation error injected into the simulation model. The position errors were evaluated as a horizontal and vertical component. The physical principles behind GPS yield better resolution in the horizontal plane than are possible for the altitude measurement. Figure 5 shows the vertical error over time. Table 4 below contains the standard deviations for the horizontal and vertical errors in feet. The horizontal errors were not modeled, due to the problem's negligible sensitivity to such small horizontal errors (as with surge, above, horizontal errors get scaled by the tangent of the 3.5 degree glideslope (~0.06)). Consequently, horizontal navigation errors resulted in altitude errors on the order of 0.03 ft, which were dismissed as insignificant. Its influence was consequently not modeled.

Table 4 : Standard Deviation of JPALS Errors

JPALS Error Component	Horizontal	Vertical
Standard deviation (ft)	0.2939	0.6467

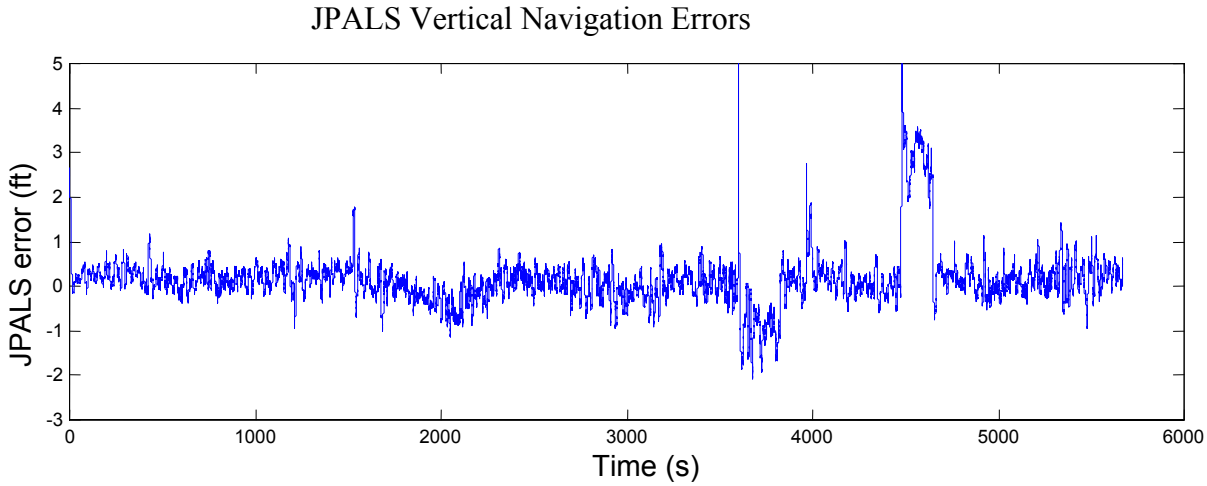

Figure 5: JPALS Vertical Navigational Error

Frequency analysis with Fourier series transforms and windowed Fourier transforms was performed to identify any frequency dependence of the JPALS error signal. No frequency dependence was noted, indicating superb blending of the GPS and INS data in a complementary filter. Although there are some transient characteristics in the navigation error, an uncolored model was deemed sufficient and used for simplicity. Consequently, the modeled navigational error signal was a normally distributed random number with the standard deviation shown above.

DRYDEN GUST

The Dryden gust model is the industry standard atmospheric turbulence model, as stipulated by the military flying qualities specification, MIL-STD-8785C. The model utilizes a

white noise source (a Gaussian distributed random number) filtered by a second-order system. The matrices below provide the gust filter.[8]

$$\dot{u}_g = \left[-\frac{V}{L_g} \right] u_g + \left[\sigma_{u_g \sqrt{\frac{2V}{L_g}}} \right] w_1 \tag{1.13}$$

$$\begin{bmatrix} \dot{w}_g \\ \dot{w}_g^w \end{bmatrix} = \begin{bmatrix} 0 & 1 \\ \frac{-V^2}{L_g^2} & -2\frac{V}{L_g} \end{bmatrix} \begin{bmatrix} w_g \\ w_g^w \end{bmatrix} + \begin{bmatrix} \sigma_{w_g} \sqrt{\frac{3V}{L_g}} \\ (1-2\sqrt{3})\sigma_{w_g} \sqrt{\left(\frac{V}{L_g}\right)^3} \end{bmatrix} w_3 \tag{1.14}$$

The graph below is a sample turbulence field behind the ship. The gust intensity increases with altitude then becomes constant. The intensity also increases with the average wind velocity. The gust field below models a 20-knot average wind speed at an altitude of 50 meters. The gust data was generated by similarly converting the above continuous time system of equations into discrete time difference equations, with a ten-millisecond time step, identical to the aircraft simulation.

[8] Mulder and Van der Vaart, "Lecture Notes Dictaat D-47: Aircraft Response to Atmospheric Turbulence," p. 209-10.

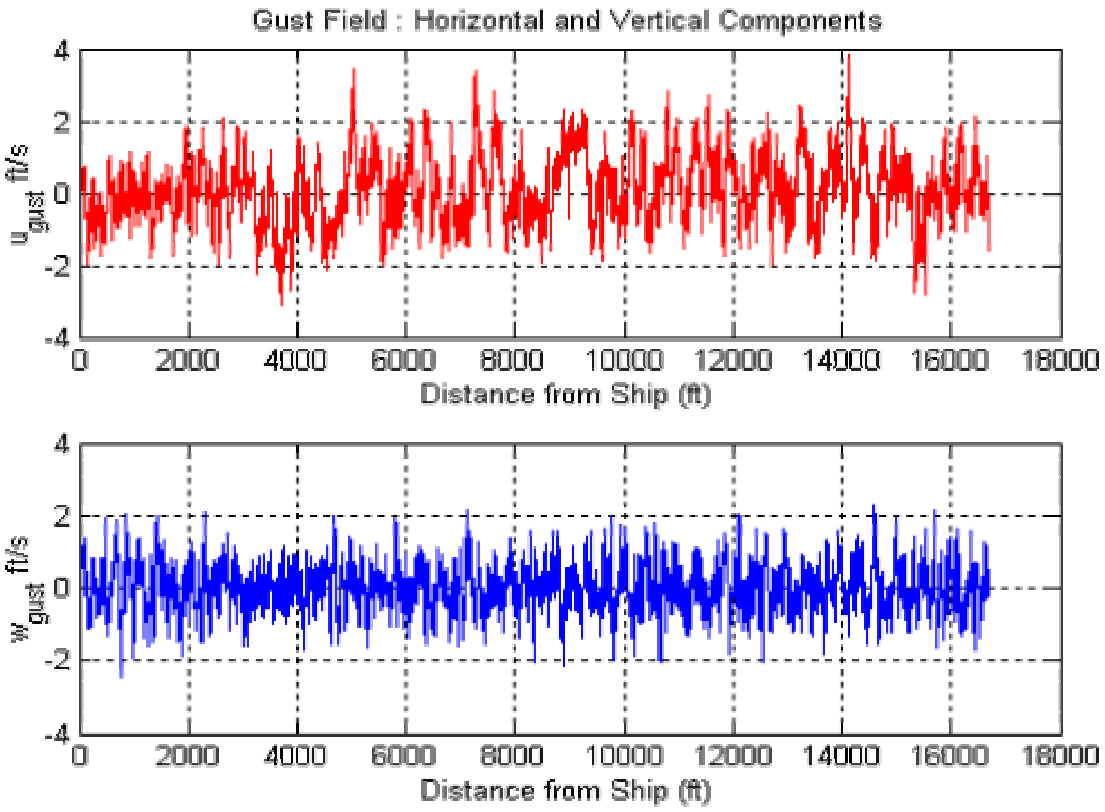

Figure 6: Model Generated Gust Field

AIRCRAFT DYNAMICS

Longitudinal aircraft dynamics can be characterized by a system of four linear differential equations, in a state-space formulation. The matrix equation 1.15 shown below is written as perturbations from the trim condition for the longitudinal states[9]. Additional states, *x*, the distance aft of the ship, and *h*, altitude were added, whose derivatives were linear combinations of the primary states.

$$\begin{bmatrix} \Delta\dot{u} \\ \Delta\dot{w} \\ \Delta\dot{q} \\ \Delta\dot{\theta} \end{bmatrix} = \begin{bmatrix} X_u & X_w & 0 & -g \\ Z_u & Z_w & u_0 & 0 \\ M_u + M_{\dot{w}}Z_u & M_w + M_{\dot{w}}Z_w & M_q + M_{\dot{w}}u_0 & 0 \\ 0 & 0 & 1 & 0 \end{bmatrix} \begin{bmatrix} \Delta u \\ \Delta w \\ \Delta q \\ \Delta\theta \end{bmatrix} + \begin{bmatrix} X_\delta & X_{\delta_T} \\ Z_\delta & Z_{\delta_T} \\ M_\delta + M_{\dot{w}}Z_\delta & M_{\delta_T} + M_{\dot{w}}Z_{\delta_T} \\ 0 & 0 \end{bmatrix} \begin{bmatrix} \Delta\delta \\ \Delta\delta_T \end{bmatrix} \quad (1.15)$$

[9] Nelson, Robert C. *Flight Stability and Automatic Control,* p. 149.

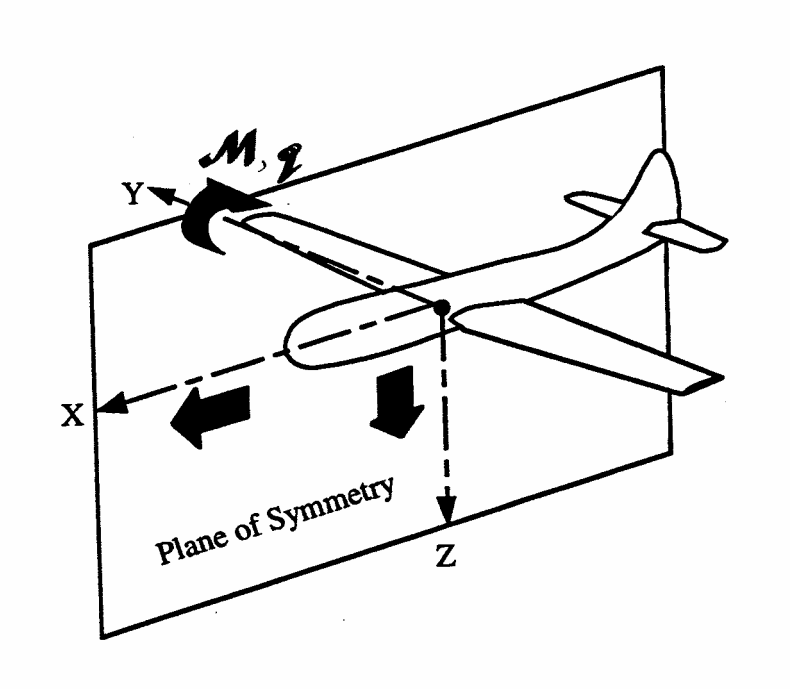

Figure 7: Aircraft Sign Conventions and Notation[10]

Figure 7 shows the accepted aircraft sign conventions and notations where: [X, Y, Z] are components of the aerodynamic force; M is the pitching moment, and q is the pitch rate.

CONTROL STRUCTURE

Design of the automatic control architecture was crucial because the control structure determines how the aircraft responds to its conditions. This means the control system is largely responsible for the aircraft landing performance. A single control structure was used to limit the study's degrees of freedom and isolate the difference in performance attributable to the aircraft parameters under investigation.

The two values we elected to track were airspeed and altitude. The controller was required to simultaneously maintain the desired airspeed and track the commanded altitude as

[10] USNTPS-FTM-No. 103, "Fixed Wing Stability and Control: Theory and Flight Test Techniques".

precisely as possible. Airspeed regulation was important for the structural and aerodynamic implications cited above. Precise altitude control was necessary to meet the landing touchdown dispersion requirement. To accomplish these, integral tracking on airspeed was required to maintain approach speed and AOA (regulating one has the effect of regulating both, due to their mathematical relationship). Integral tracking was also required on altitude to track the glide slope, which the controller viewed as a ramp input (With altitude as a state, the system was Type-1. The additional integrator was required to achieve zero steady-state error in response to a pure ramp input.).

Sensors are also important because any feedback control system depends upon measured values for its calculation of control deflections. All aircraft states were reasonably assumed known and available for state feedback from commonly installed production aircraft instrumentation. The only modeled sensor errors were the JPALS navigation errors.

Development of a suitable control architecture proved to be difficult. Specifically, the thorny problem was determining a control architecture that would permit the controller to take advantage of the known ship pitch and heave rates to track a command composed of the superposition of a ramp and a complex sinusoidal. These values are reasonably known from ship-based accelerometers and rate gyros, and capable of providing lead compensation to improve the ability of the airplane to track a pitching, heaving deck. The particular challenge was implementing lead compensation in a state-space formulation. This was done using the Delta-implementation model devised by Kaminer.[11] Though originally introduced for the purpose of improving the robustness of gain-scheduled controllers, it also resolved our problem of using the altitude error rate to provide lead tracking. The Delta-implementation involves conceptually

[11] Kaminer, "A Velocity Algorithm for the Implementation of Nonlinear Gain-Scheduled Controllers", *Automatica*, Vol. 31, pp. 1185--1191.

placing a differential prior to multiplication by feedback gains and then subsequent integration. In our case the implementation is depicted below in Figure 8. In lieu of the differential block below, the measured altitude error rate would be injected directly from the sensors.

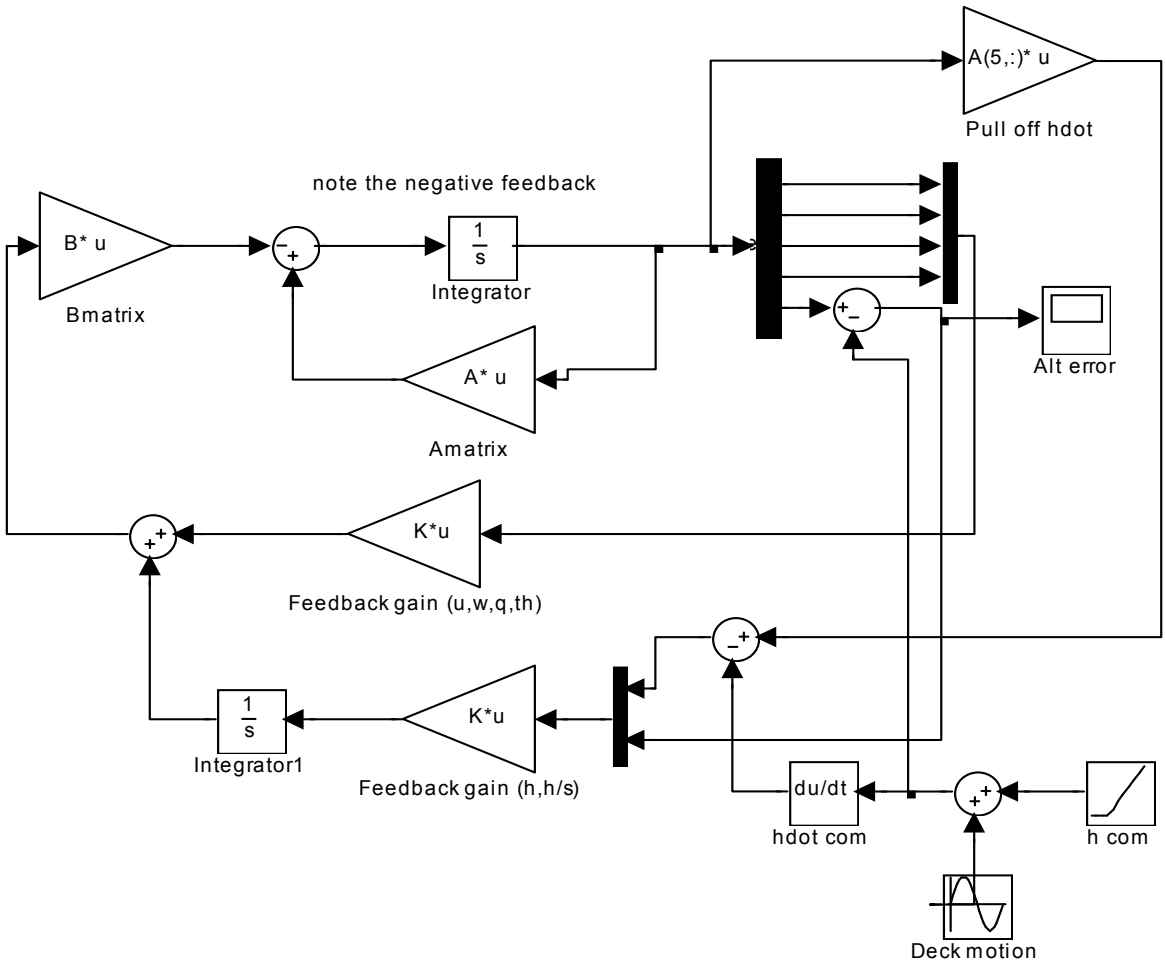

Figure 8: Implementation Model for State Feedback Controller using Kaminer's Delta Method

In Figure 8 the aircraft dynamics are represented by the B matrix and the A matrix in a loop with an integrator. The rest of the diagram depicts the control system's various feedback loops including integral action utilizing ship rate information to zero the tracking error for a

ramp input. The derivative feedback provides lead compensation to improve the tracking of the complex sinusoidal deck motion.

A simplified graphical representation of the system used to implement the gains is shown in Figure 9. In this case the outputs of interest are velocity perturbation and altitude error. The bottom two gains add integral action to the altitude error and velocity perturbation respectively, which regulates those signals to zero. Every perturbation state has an influence on both the elevator and throttle commands weighted by their individual gain constant. These products are then added to determine the control commands.

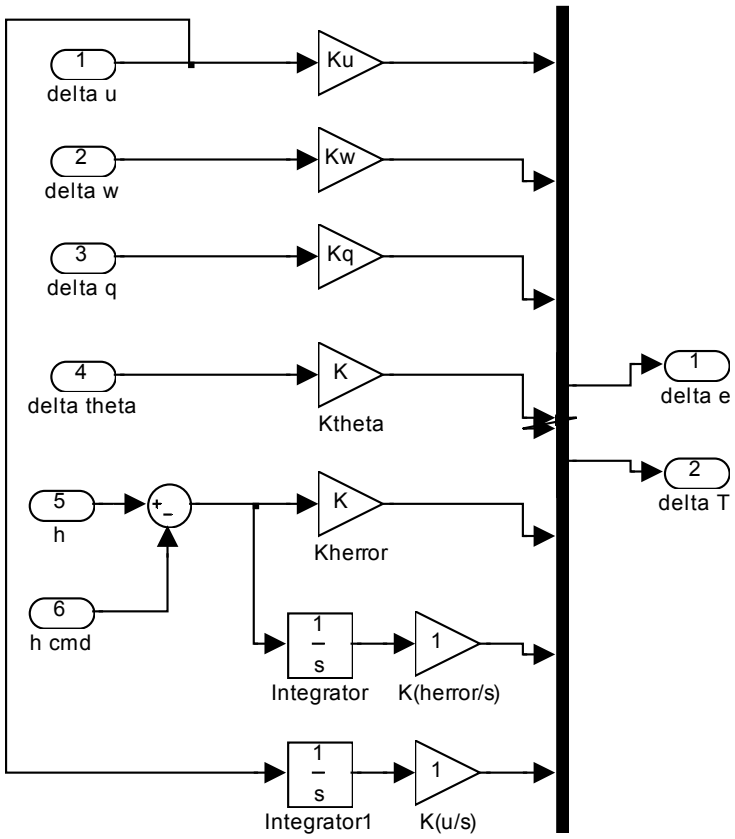

Figure 9: Graphical Depiction of Control Structure Implementation

Figure 9 depicts the aircraft states being multiplied by their respective gains and summed for the resulting elevator and throttle commands. These gains were calculated by the `'lqry'` function in MATLAB, which is a linear quadratic regulator (LQR) with output weighting. The `lqry` command calculates state-feedback gains to minimize a cost function, provided as equation 1.15, for the specified system and weightings; however, the implementation system and the system for gain calculations are not the same. The difference is the gains are calculated for h and $\frac{h}{s}$ making it a regulator problem, but the implementation used h_{error} and $\frac{h_{error}}{s}$ transforming it to a tracking problem. The matrix Q weights the output states, and R weights the control inputs.

$$J = \int_0^\infty \left(\bar{y}^T Q \bar{y} + \bar{\eta}^T R \bar{\eta} \right) dt \tag{1.16}$$

The output, $\bar{y}$, was composed of the elements given in equation 1.17 below. The effect is to place two zeros in the open-loop transfer function, which attract the closed-loop poles. Zero locations were determined by brief trial and error, attempting to minimize the observed tracking error without excessive control activity.

$$\bar{y} = \begin{bmatrix} \left(s + 3 + \frac{3}{s} \right) h \\ \left(1 + \frac{0.5}{s} \right) u \end{bmatrix} \tag{1.17}$$

With complete synthesis model, including the integral action on both altitude and airspeed and the output weighting is depicted in equation (1.18) below.

$$\frac{d}{dt}\begin{bmatrix} u \\ w \\ q \\ \theta \\ h \\ h/s \\ u/s \end{bmatrix} = \begin{bmatrix} X_u & X_w & 0 & -g & 0 & 0 & 0 \\ Z_u & Z_w & u_0 & 0 & 0 & 0 & 0 \\ M_u + M_{\dot{w}} Z_u & M_w + M_{\dot{w}} Z_w & M_q + M_{\dot{w}} u_0 & 0 & 0 & 0 & 0 \\ 0 & 0 & 1 & 0 & 0 & 0 & 0 \\ 0 & -1 & 0 & u_0 & 0 & 0 & 0 \\ 0 & 0 & 0 & 0 & 1 & 0 & 0 \\ 1 & 0 & 0 & 0 & 0 & 0 & 0 \end{bmatrix} \begin{bmatrix} u \\ w \\ q \\ \theta \\ h \\ h/s \\ u/s \end{bmatrix}$$

$$+ \begin{bmatrix} X_{\delta_e} & X_{\delta_T} \\ Z_{\delta_e} & Z_{\delta_T} \\ M_{\delta_e} + M_{\dot{w}} Z_{\delta_e} & M_{\delta_e} + M_{\dot{w}} Z_{\delta_T} \\ 0 & 0 \\ 0 & 0 \\ 0 & 0 \\ 0 & 0 \end{bmatrix} \begin{bmatrix} \Delta\delta_e \\ \Delta\delta_T \end{bmatrix}$$

$$y = \begin{bmatrix} 0 & -1 & 0 & u_0 & 3 & 3 & 0 \\ 1 & 0 & 0 & 0 & 0 & 0 & 0.5 \end{bmatrix} * \begin{bmatrix} u \\ w \\ q \\ \theta \\ h \\ h/s \\ u/s \end{bmatrix} \tag{1.18}$$

For our problem, the weight values of Q and R were determined using the method suggested by Nelson[12], whereby the individual diagonal elements of Q and R were the reciprocals of the desired relative magnitudes. The weights were constant throughout all controllers used in the trial. No attempt was made to optimize controller performance by tuning Q and R. The purpose was to ensure that the effects of airframe attributes were not masked by variances in controllers as discussed above.

[12] Nelson, Robert C. *Flight Stability and Automatic Control,* p. 386ff.

LANDING SIMULATIONS

Simulations were conducted to determine the influence of three aircraft attributes on landing performance; namely lift curve slope, longitudinal stability, and drag coefficient using the A-4D as a test frame. These attributes were selected because Heffley's study for manned performance specifications indicated these characteristics had the most influence on a pilot's ability to land[13].

The A-4D was selected as the baseline airplane because of its similarity in weight and basic geometry to current and proposed UCAV projects. Data (weights, inertias, stability derivatives, airspeeds) were used with the A-4D configured for landing: gear and flaps down. The simulation code included in Appendix I automatically ran one hundred thousand landing simulations with the specified disturbance conditions. These simulations were split evenly between one hundred aircraft configurations covering the full range of possible combinations of lift curve slope and longitudinal stability, storing the key results from each run. A second version of the code was used to simulate combinations of lift curve slope and drag coefficient. The only difference was the variable in the outer loop as described below.

The simulation code was organized as a cascade of nested loops. First, the ship states were loaded for the desired sea-state and used to calculate the position of the landing surface and its rate as a function of time. Many basic parameters were defined, the gust model was calculated and stored as a discrete time system; its random number seed was initialized with the clock to guarantee a unique set of conditions for every simulation. The above calculations were performed only exterior to all loops. Next, the two outermost loops varied two aircraft attributes from low to high by nine uniform increments to test a comprehensive grid of one

[13] Heffley, *Outer-Loop Control Factors For Carrier Aircraft*.

hundred possible combinations. The discrete time system and the feedback gains for each specific aircraft configuration were calculated. Third, an intermediate loop initialized one thousand trials for each configuration by positioning the aircraft on the glide slope six thousand feet behind the ship, generating a unique gust field, generating a random normal distribution of navigation errors, and randomly selecting the initial ship condition. Fourth, the inner-most loop executed each individual simulation run, culminating in a landing, with the aircraft states and control positions updated one hundred times per second (i.e. 10 msec intervals). Some post-processing was done and important values were archived. Results were saved after every one thousand simulations, to prevent excess time loss in the event of a program crash. The stored data required additional post-processing to produce most of the desired plots.

Each of these sets of 100,000 simulation runs was then repeated for varying sea-states, wind conditions, actuator dynamics, and the cross dependencies of airplane aerodynamic attributes. The following table lists the test conditions.

Table 5: All Simulated Test Conditions

Attributes Varied		Sea-state	Wind Velocity (knots)	Navigation Errors
$C_{l\alpha}$	$C_{m\alpha}$	3	20	on
$C_{l\alpha}$	$C_{m\alpha}$	4	40	on
$C_{l\alpha}$	$C_{m\alpha}$	5	20	on
$C_{l\alpha}$	C_{Do}	3	20	on
Baseline		3	off	off
Baseline		4	off	off
Baseline		5	off	off
Baseline		off	20	off
Baseline		off	off	on
Baseline		3	20	on
Baseline		4	20	on
Baseline		4	40	on

RESULTS AND DISCUSSION

The following discussion progresses from analysis on single simulation runs, through the influence and sensitivity to the three sources of disturbances, to specific conclusions bounding suitable aircraft characteristics based on statistics from many simulations. The primary figures of merit are the boarding rate and landing dispersion requirements previously presented in Table 1. Secondary figures of merit derived from other structural and actuator limits, including RMS control power and standard deviation of pitch angle, are also discussed. The influence of three aircraft characteristics, namely lift-curve slope, longitudinal stability, and coefficient of drag on these performance metrics were analyzed. For ease of interpretation, all graphics in this section are standardized such that desirable performance is in the direction of the blue and undesirable performance is in the direction of the red.

SINGLE SIMULATION RUNS

PRELIMINARY RESULTS (LQR)

Initially a LQR controller was used to establish performance trends and implement the three disturbance sources, while working on a more advanced control architecture. Figure 10 shows the flight path time history for one preliminary simulation at sea-state 3. The top portion depicts the commanded and actual altitude as time progresses from left to right. The middle portion shows the deck altitude in blue and the aircraft's altitude error in red. Note the altitude error is actually larger than the ship motion. This was due to the control system lag.

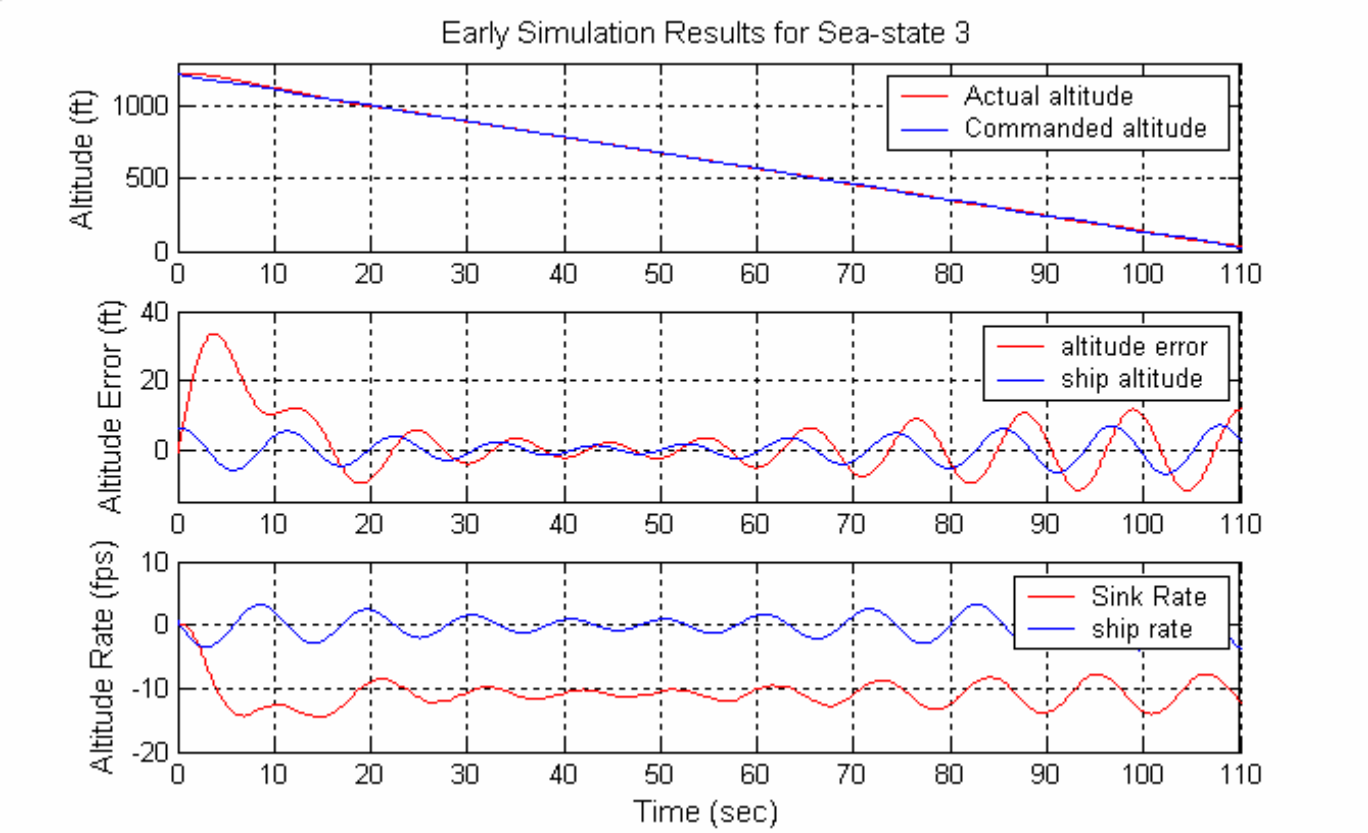

Figure 10: Preliminary Single Simulation Flight Path and Error

This magnitude of error was unacceptable. An altitude error of 10 feet mapped onto the landing area produces a landing error of 163.5 feet. Although the performance was so poor that no further results will be presented, several trends were established. The LQR controller was sensitive to sea-state, but performed very well when only the navigation and gust error sources were turned on. Lift curve slope was shown to be the dominant factor in landing performance while longitudinal stability and drag had little to no effect. Also, the effects of bandwidth limits on the control actuators were tested. Landing performance decreased as actuator speed decreased, but the reduction in performance was small even with tight bandwidth limits.

FINAL CONTROL STRUCTURE (LQRY)

The implementation of a control structure that utilized ship rate dramatically improved landing performance. The linear quadratic regulator algorithm with output weighting (`'lqry'`) was used to determine state-feedback gains. Figure 11 illustrates the same information using this controller at sea-state 5 that Figure 10 illustrates for sea-state 3, with an additional line depicting the altitude error rate. The middle portion of Figure 11 shows that despite a 2.5-fold increase in deck motion, the altitude error was reduced by about 60%.

Note that the altitude error has the same sign as the deck displacement. This signifies two things. First, the aircraft's altitude was changing more than the commanded altitude. Second, when the ship was pitched nose down the aircraft was generally above the commanded altitude, which increased the hook-to-ramp distance and helps account for the absence of landings short enough to require a waveoff. This safety margin would otherwise be reduced when the ship is pitched nose down because the flight-path angle relative to the deck is the flight-path angle relative to the horizon minus the ship's pitch angle.

Figure 12 illustrates the gust intensity, the control response, and selected aircraft states for the same simulation run. Several important features of this control structure were noted when evaluating Figures 11 and 12 together. First, the throttle command follows the ship rate with a slight lead. This is the lead compensation achieved with Kaminer's Delta method. Second, the throttle command handled mostly the low frequency task of tracking the ship motion while the elevator handled the high frequency task of correcting for gusts. Note the stable platform caused the elevator command to track the ship motion as well. Third, the AOA variations were small. This is important for stall margin considerations and validates the assumed linearity (Recall this study used a linear model; therefore stall effects were not included.).

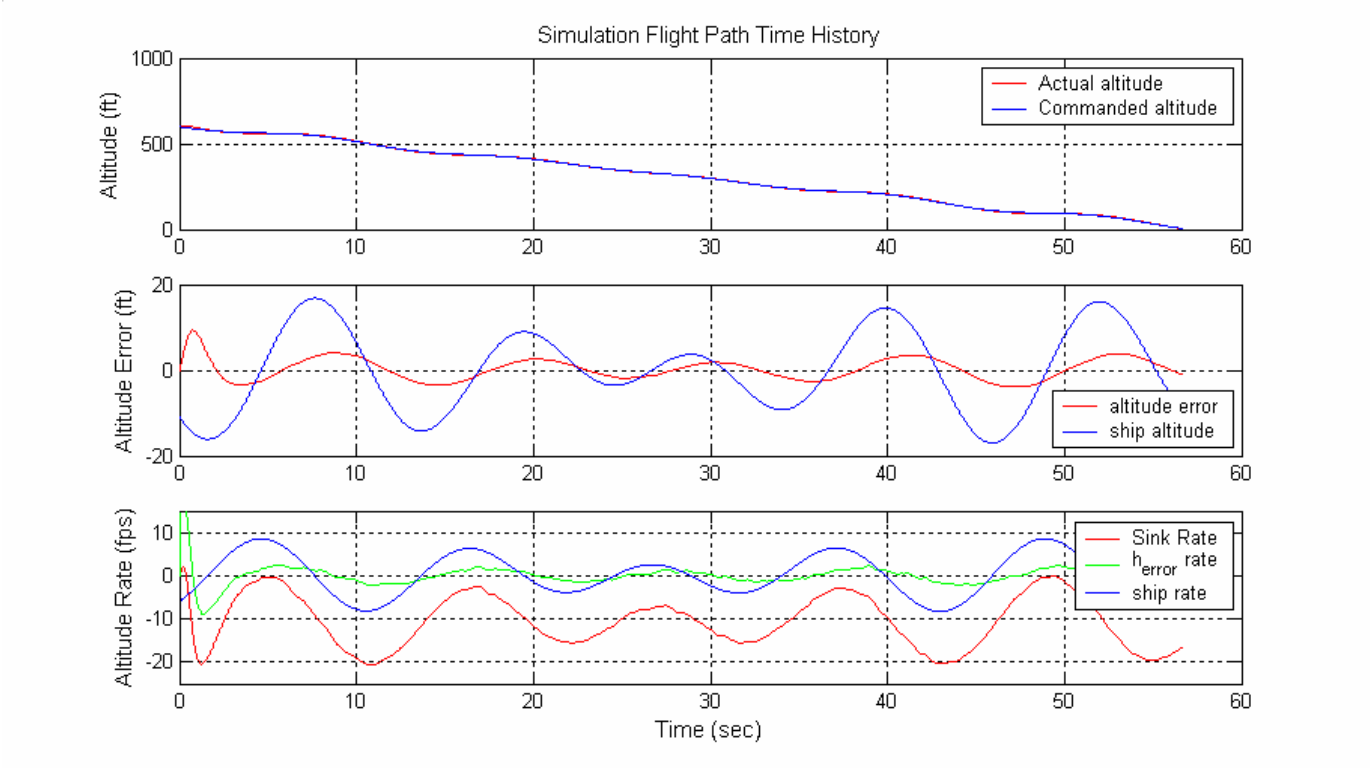

Figure 11: Flight Path History at Sea-state 5

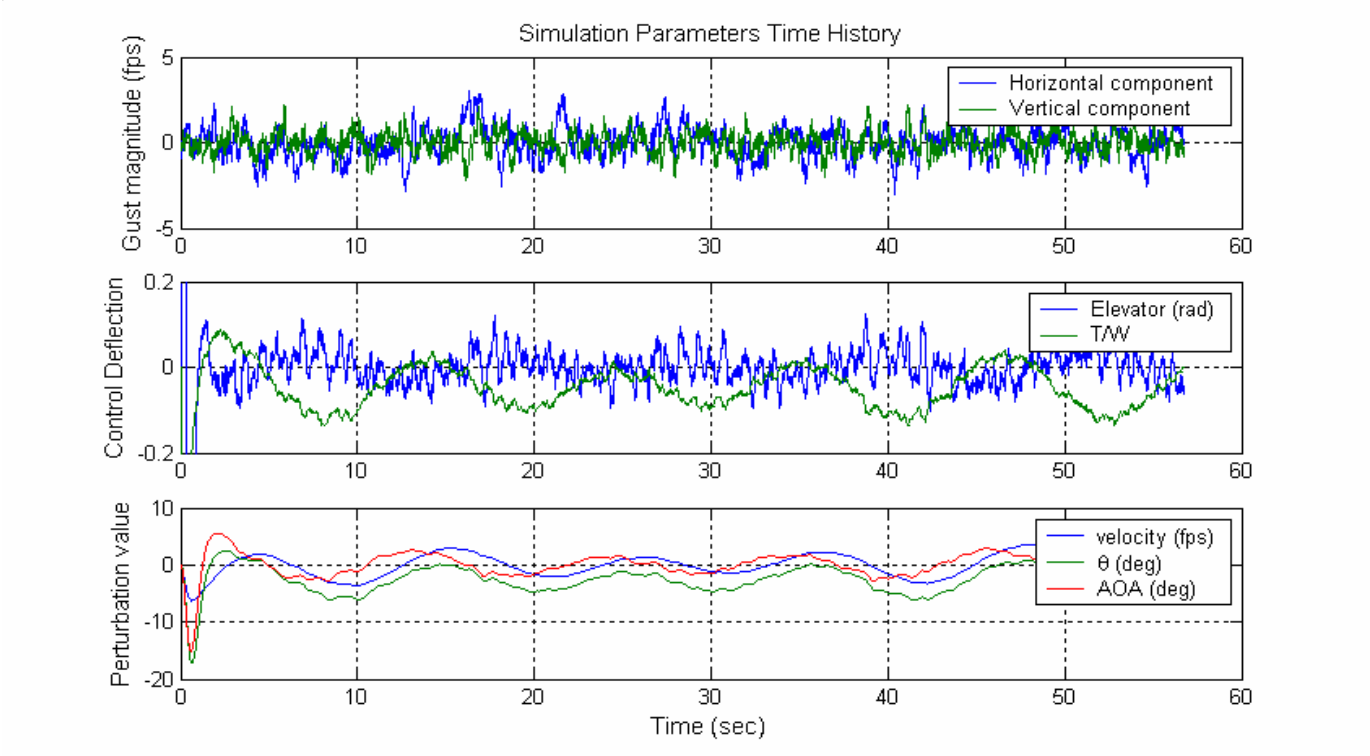

Figure 12: Disturbances' Influence on Aircraft States

DISTURBANCE SOURCES

First, it was important to understand the effects of each source of noise on landing performance. To do this, five hundred simulations were run with baseline A-4D characteristics[14] with each source of noise individually. All other simulations were run with all three sources of error turned on. Figure 10 shows these simulation results. The upper bound for sea-state 5, which is off the top of the graph, was 203 ft. Figure 13 clearly demonstrates that ship motion was the dominant source of landing error. Sea-state 5 was the most demanding case because of the magnitude of the required flight path changes. The deck moved as much as thirty four feet vertically in ten seconds, challenging the system's ability to track a command.

Figure 13 also shows landing dispersion and bounds were highly sensitive to sea-state. Landing dispersion increased only slightly with wind velocity, but the bounds increased nearly linearly. Navigation errors resulted in a dispersion and range between those for ten and twenty

[14] McRuer, *Aircraft Dynamics and Automatic Control,* p700ff.

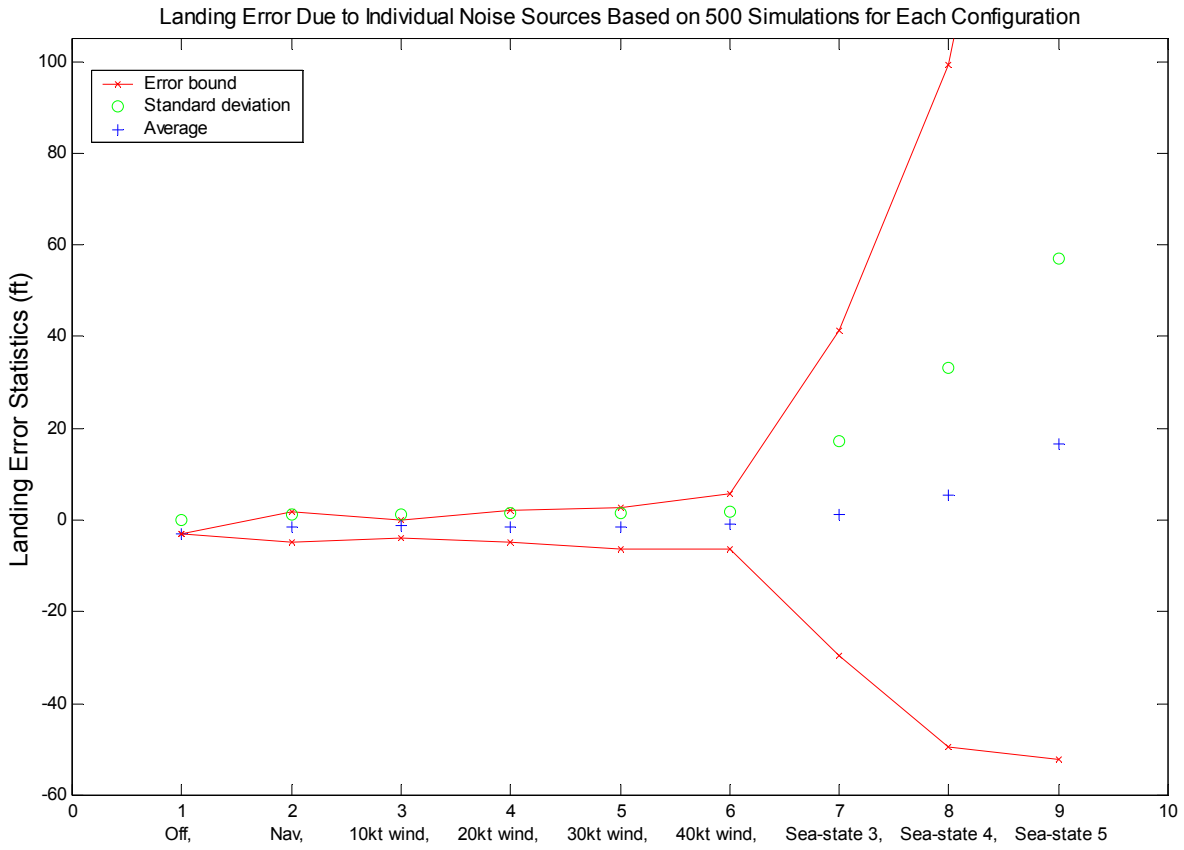

Figure 13: Landing Position Error Statistics for Each Noise Component

knots of wind. Additional tests were conducted for the baseline A-4D to determine how the three disturbance sources interact. Table 5 shows that the addition of gusts and navigation errors has negligible influence on the landing dispersion and landing position error range from sea-state alone. The variability due to the phase of ship motion from one set of five hundred simulations to the next caused greater influence on landing statistics than the addition of gust and navigation errors. Therefore results from a simulation model that accounts only for ship motion would be legitimate.

Table 6: Combination Effects of Disturbance Sources

Condition	Std. Dev (ft)	Error Range (ft)
Sea-state 3	17.4	70.8
Sea-state 4	33.2	148.8
Sea-state 3, 20wind, nav	17.3	72.7
Sea-state 4, 20wind, nav	33.7	147.0
Sea-state 4, 40wind, nav	33.1	151.8

INFLUENCE OF LIFT CURVE SLOPE AND LONGITUDINAL STABILITY

The combined influence of longitudinal stability and lift curve slope was evaluated by a combined total of three hundred thousand simulation runs. The lift curve slope was varied from six-tenths per radian to six per radian in increments of six-tenths per radian. Lift curve slope varies with wing sweep angle and aspect ratio, with lower values of aspect ratio and aft wing sweeps resulting in lower values of lift curve slope. The longitudinal stability was varied from negative sixty-five hundredths (stable) to twenty-five hundredths (slightly unstable) in increments of one tenth. Longitudinal stability is dependent on the location of the center of gravity relative to the wing's aerodynamic center, where moving the center of gravity aft decreases stability. All other attributes were those for the baseline A-4D in the landing configuration, including a lift to drag ratio of approximately two. At each combination, one thousand simulated landings were performed for each sea-state and the landing statistics captured as discussed previously.

BOARDING RATE AND LANDING DISPERSION

The sea-state 3 simulations for all modeled configurations had error bounds within the acceptable landing area. This means that if landing position were the only criterion, the autonomous system would have a perfect boarding rate for any aircraft for all conditions up to

and including sea-state 3. Sea-state 3 simulation results yielded no further information and are not shown.

The boarding rate for sea-states 4 and 5 are plotted below in Figures 14 and 15, each has lift curve slope increasing up the y-axis and stability decreasing along the x-axis. Sea-state 4 was run with forty-knot average wind speed, while sea-state 5 was run with twenty-knot wind. Note these boarding rates account only for landing position and do not account for the possibility of extreme touchdown attitudes at which arrestment would be unsuccessful.

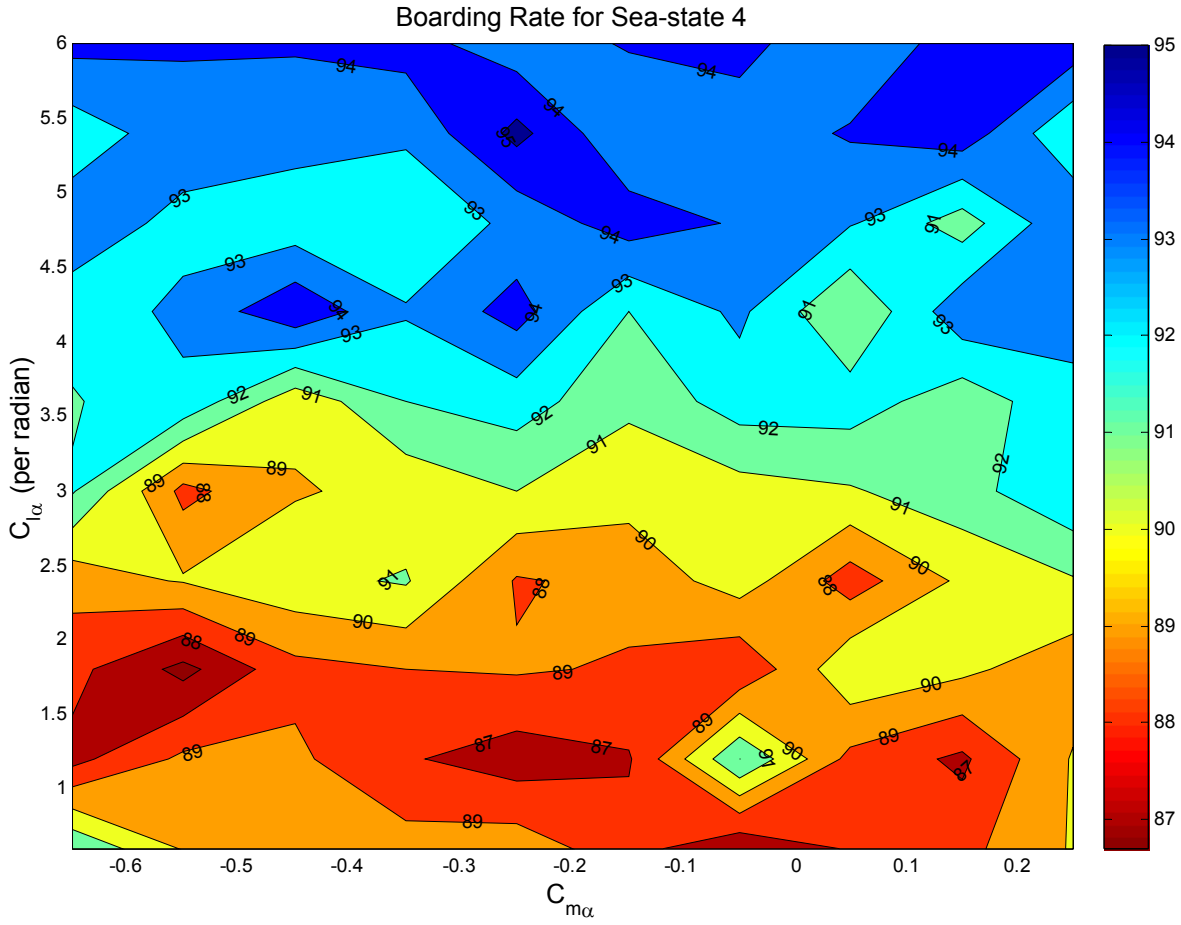

Figure 14: Sea-state 4 Boarding Rate Contour

Figure 14 illustrates the boarding rate for sea-state 4 ranges from the high eighties to the mid nineties depending on the aircraft parameters. In general, higher lift curve slopes provide higher boarding rates, while longitudinal stability has little effect. The lack of smooth contours was attributed to insufficient sample size to fully capture the variability in the ship motion. Figure 15 shows the same trends more smoothly for sea-state 5 with boarding rates from the mid seventies to low eighties. In all, two hundred thousand simulations at sea-state 4 and 5, only one failed to land because it was too short. This is an important safety result. Short landings are dangerous because of the risk of a "ramp strike" or crashing into the back of the ship.

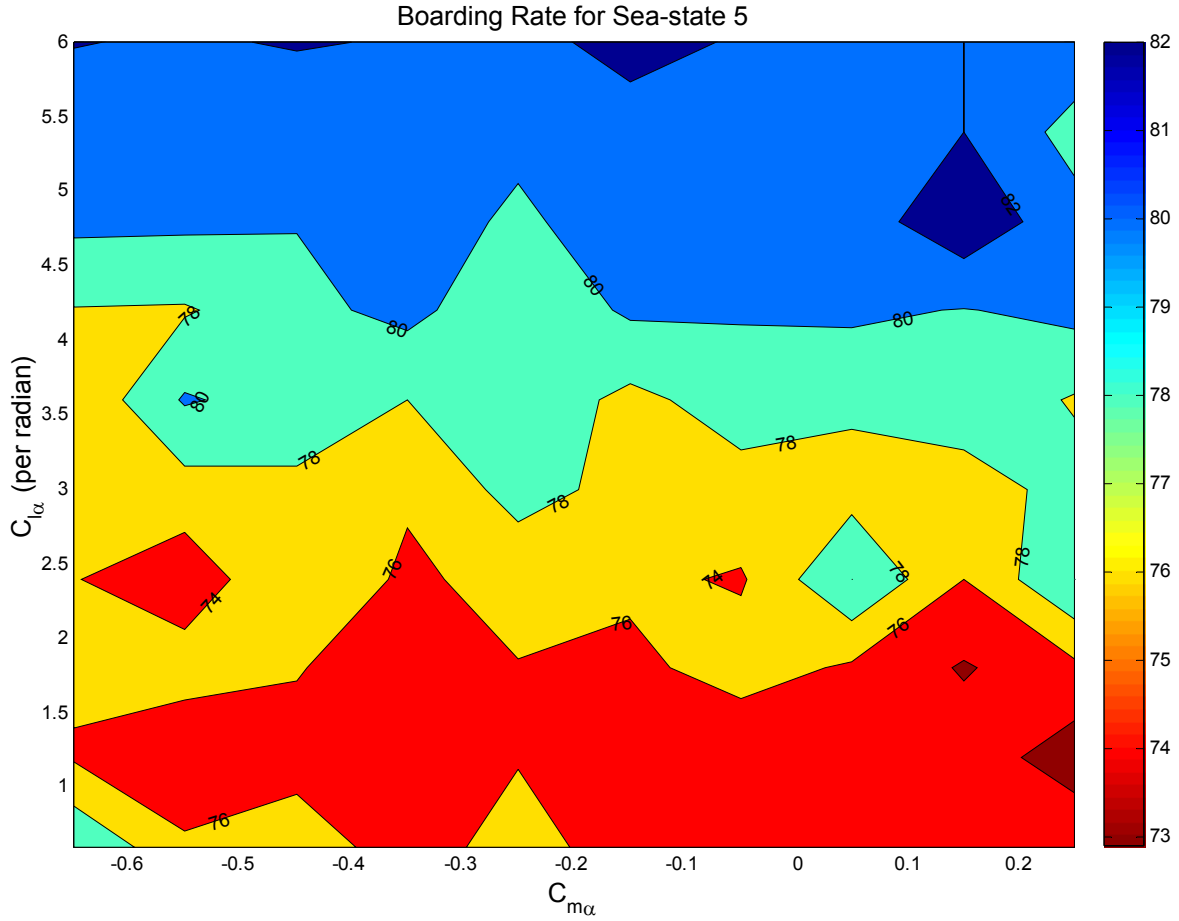

Figure 15: Sea-state 5 Boarding Rate Contour

Boarding rates are strongly related to the landing dispersion. Figure 16 depicts the landing dispersions for the most demanding case, sea-state 5. Recall the required performance presented in Table 1 was a standard deviation of sixty feet or less. This requirement is satisfied for all configurations in the blue portion of Figure 16. A lift curve slope of 2.5 per radian or greater is required depending on the aircraft stability. For perspective, the A4-D has a relatively low lift curve slope of 3.5 per radian while the Boeing 747 has a high lift-curve slope of 5.7 per radian[15].

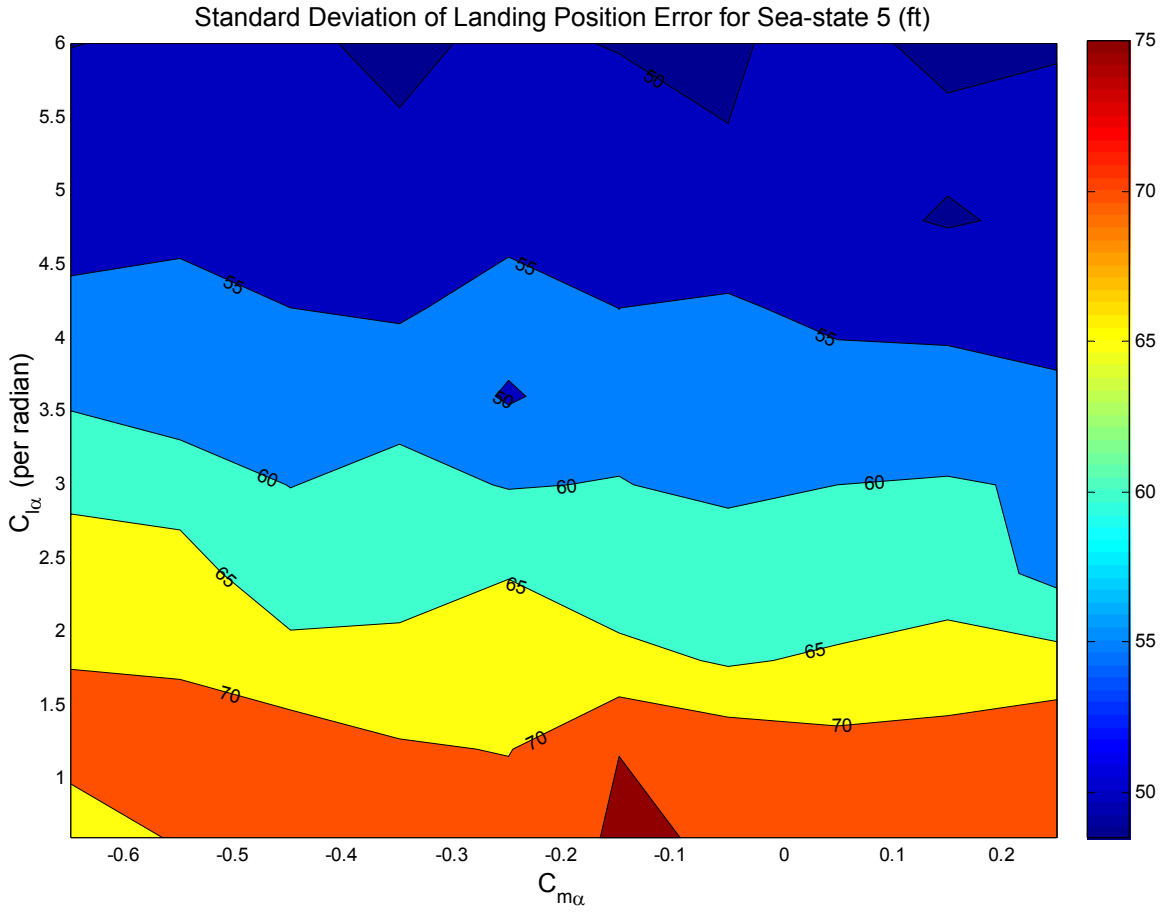

Figure 16: Sea-state 5 Landing Position Error Standard Deviation Contour

[15] Nelson, Robert C. *Flight Stability and Automatic Control,* p. 416.

The boarding rates presented in Figure 15 are higher than expected for the landing dispersions shown in Figure 16. This is because the simulated landings are not normally distributed. Figure 17 illustrates the actual landing distribution for five hundred simulations with the baseline A4-D for sea-state 5. This was attributed to the effective ship geometry due to ship motion. When the front of the ship was pitched down, it presented a much smaller target than when pitched up or level resulting in the greater spread of long landings then for short landings.

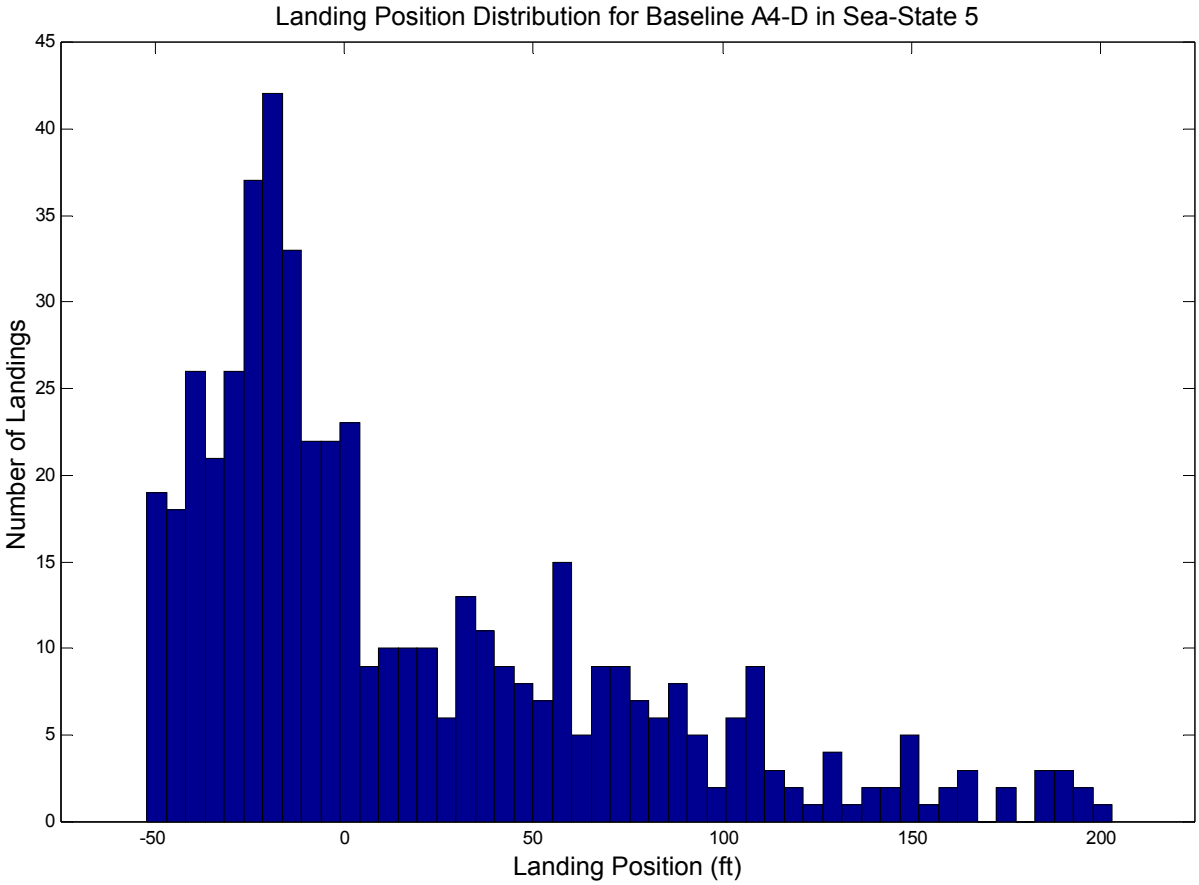

Figure 17: Sample Landing Error Distribution for Sea-state 5

Also, when the ship is pitched nose down, once the aircraft was beyond the target point, the commanded altitude was high because the altitude command was corrected for the targeted landing position not for the deck displacement at the aircraft's actual position. Five hundred

simulations were run with the commanded altitude corrected for the aircraft's actual position to test its influence on performance. The standard deviation decreased slightly and the maximum error decreased by more than ten percent, but there was no change in boarding rate, therefore previous simulations were not redone.

PITCH ATTITUDE

Landing position is not the only concern for carrier-based aircraft. The aircraft's pitch attitude must be tightly controlled to ensure the main gear touchdown first and that the hook will engage properly. Figure 18 depicts the standard deviation of pitch angle during the simulated approaches at sea-state 5. A standard deviation of two degrees satisfies the geometry constraint. Therefore, Figure 18 demonstrates the minimum acceptable lift curve slope is 2.9 per radian, which is consistent with the above requirement imposed by boarding rate and dispersion.

Constraining pitch also regulates angle of attack. Only small variations are permitted to avoid flying approach with a large stall margin, which would drive the approach speed up. As with landing precision, pitch attitudes are better for steeper lift-curve slopes with secondary effects improving with decreased longitudinal stability. Note these contour lines are smooth. This is because pitch angle was sampled thousands of times during every simulated approach compared to a single landing position collected during each simulation.

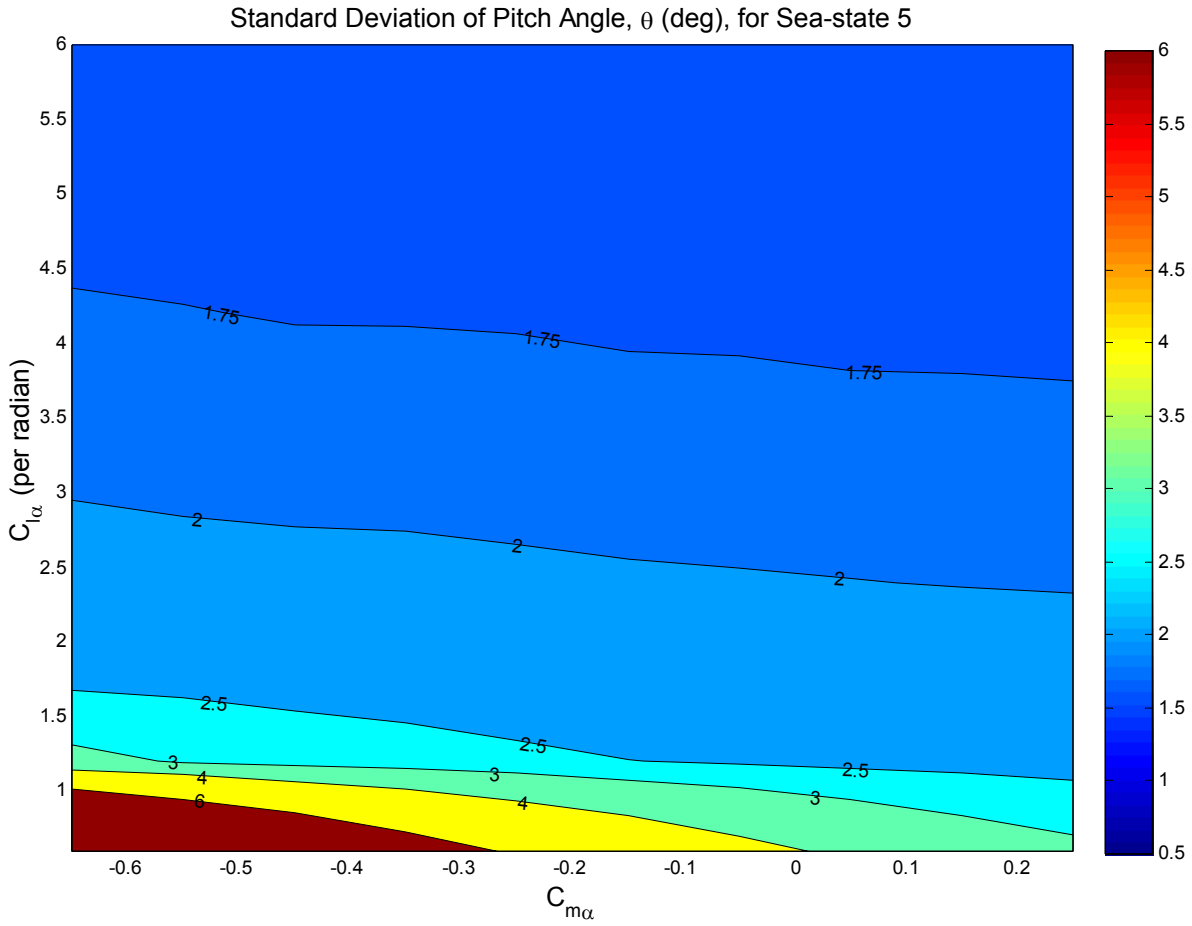

Figure 18: Sea-state 5 Pitch Angle Standard Deviation Contour

REQUIRED CONTROL POWER

Control authority is another issue for aircraft on approach. Controls are limited both in rate and magnitude. Elevators are operated by high-pressure hydraulics and can move rapidly through a wide range of angles. Highly stable platforms will require larger elevator deflections to achieve a desired change in angle of attack than a less stable platform, but will return to the desired attitude automatically when disturbed by a gust. Shallow lift-curve slopes require a greater change in angle of attack and therefore larger elevator deflections. Figure 19 depicts the RMS elevator control power during the simulated approaches at sea-state 5 with twenty-knot wind.

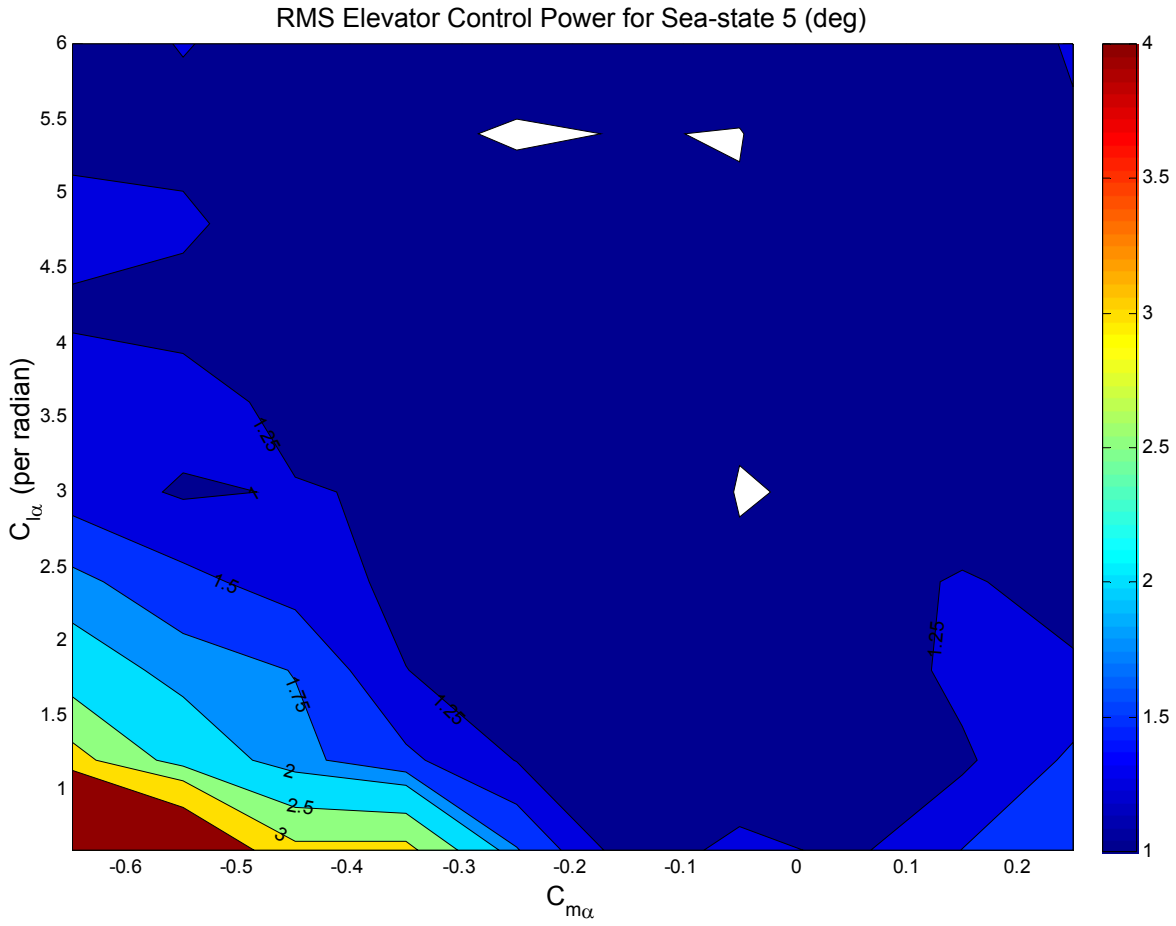

Figure 19: Sea-state 5 RMS Elevator Control Power

Figure 20 illustrates the RMS elevator power for sea-state 4 with forty-knot winds with the same color scale as Figure 19. Note the general increase in required elevator power. This indicates that the gust intensity had a greater influence on the minimum required elevator power than the sea-state condition.

Required elevator power is dependent on both lift-curve slope and the longitudinal stability. Available elevator power only limits performance for combinations with high stability and very low lift curve slopes. As with all previous metrics, increasing the lift curve slope improved performance.

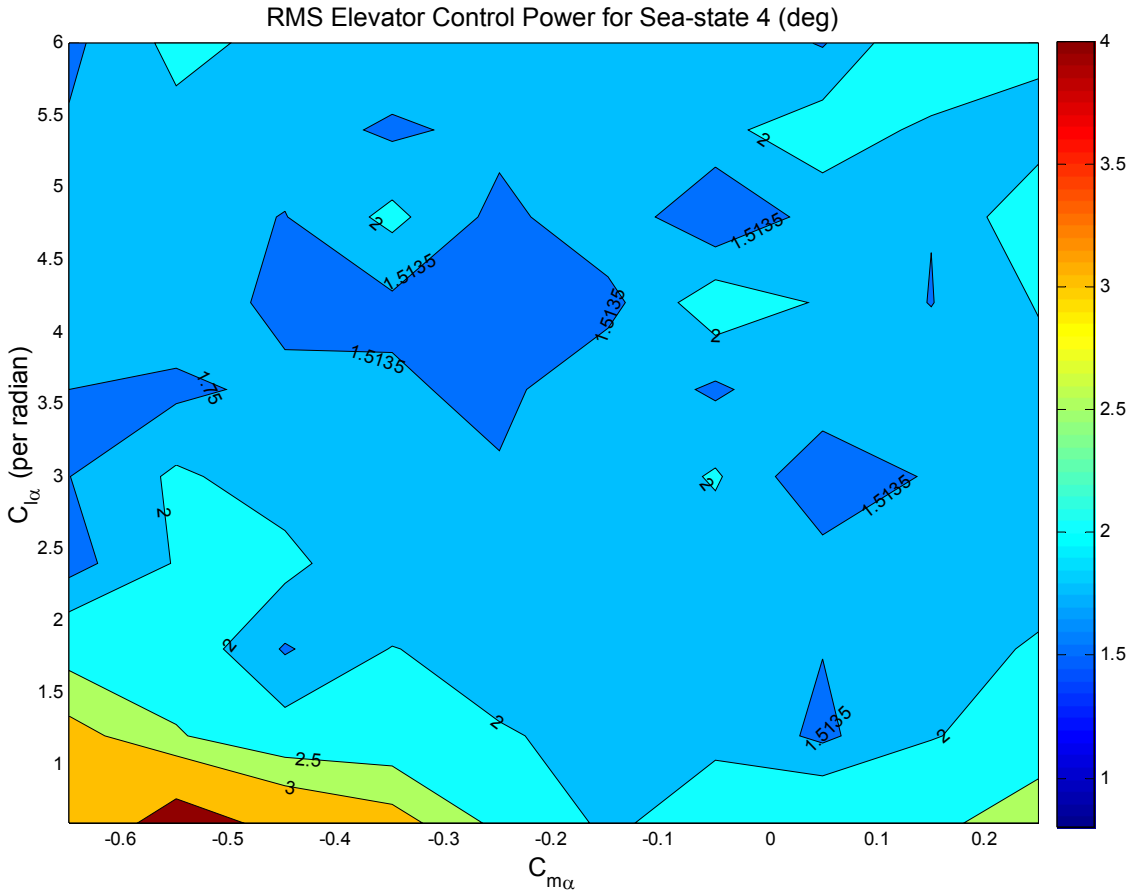

Figure 20: Sea-state 4 RMS Elevator Control Power

Throttle response is slow compared to other actuators because of the high rotational inertias of gas turbine engines. The slow engine response and transient nature of gusts and navigation errors led to less dependence on longitudinal stability. Figure 21 shows the RMS throttle control power with strong dependence on lift curve slope and minor dependence on longitudinal stability. Lower values mean less throttle activity, which is desirable.

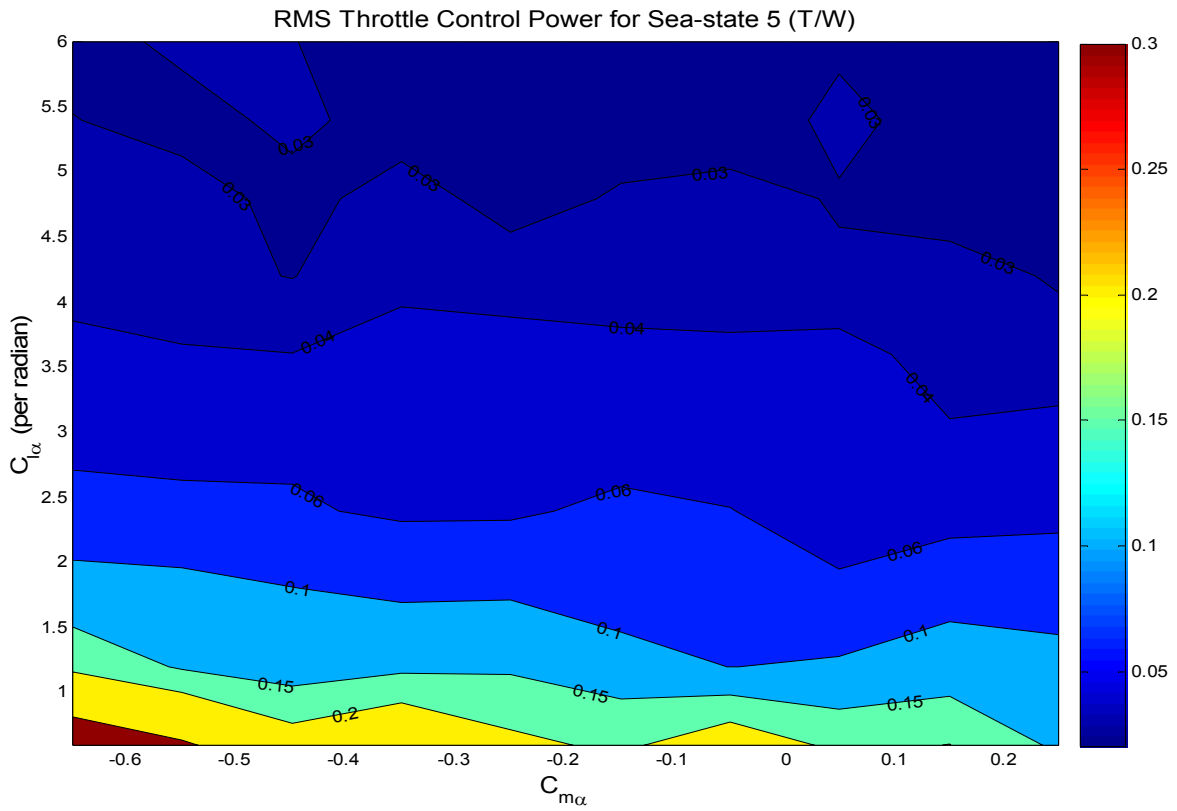

Figure 21: Sea-state 5 RMS Throttle Control Power

Figures 19 through 21 provide trend data, but are difficult to relate to familiar control values. Figure 22 below depicts a sample control history from the corners of the control power contour plots for sea-state 5. Elevator deflections are scaled in radians rather than the more familiar degrees to keep the magnitude similar to the throttle command, which is plotted as the thrust-to-weight ratio. The elevator rates and magnitudes were within normal ranges, however; the sample on the bottom left, provided for the shallow lift-curve slope with high stability, did not leave sufficient control authority for maneuvering or for trim. Half a radian is almost thirty degrees, which is a typically maximum available deflection. Similarly the throttle activity was within the normal rate limits, but the bottom left sample shows excessive required thrust magnitudes. A thrust-to-weight range of plus to minus six tenths would require a maximum

thrust to weight of at least one and three tenths without afterburner because idle thrust is typically one tenth of maximum thrust and afterburner is not permissible for approach. Plus to minus two tenths thrust-to-weight ratio is a reasonable range for approach.

Also illustrated in Figure 22, the `lqry` gain set did a surprisingly good job allocating high frequency regulation tasks to the elevator and low frequency tasks to the throttle. Notionally, the elevator can be viewed as controlling the high frequency contributions of the gusts and navigational errors, while the throttle responded to low frequency deck movement. This was not deliberate, but highly desirable. Had this not been the case, a control strategy such as eigenstructure might have been necessary in practice to prevent over-driving the throttle.

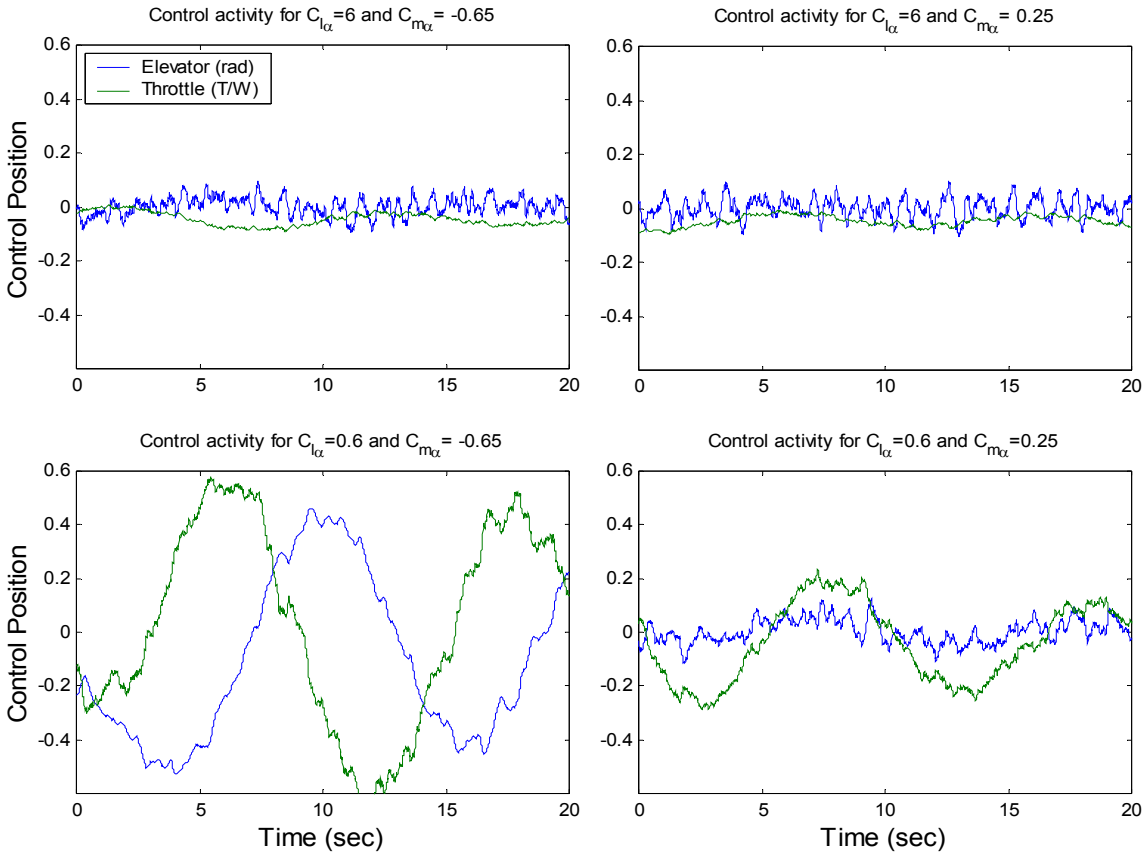

Figure 22: Sample Sea-state 5 Control Histories

INFLUENCE OF LIFT CURVE SLOPE AND DRAG COEFFICIENT

The effect of coefficient of drag on landing performance was evaluated from 0.4 to 1.075 in increments of 0.075. These values range from approximate lift to drag ratios of three down to one. The lift curve slope was varied in exactly the same manner as for the previous section, but the stability was held constant ($C_{m\alpha} = -0.41$). Again, one thousand simulations were conducted for each aircraft configuration. Only one disturbance condition was run for these configurations, namely sea-state 3 with twenty-knot wind.

Figure 23 depicts the resultant landing dispersions. As in the previous section, boarding rates were perfect for all configurations at sea-state 3. Varying the coefficient of drag had minimal effects on landing performance. Landing performance was again highly dependent on lift curve slope, which improved for increasing lift curve slope.

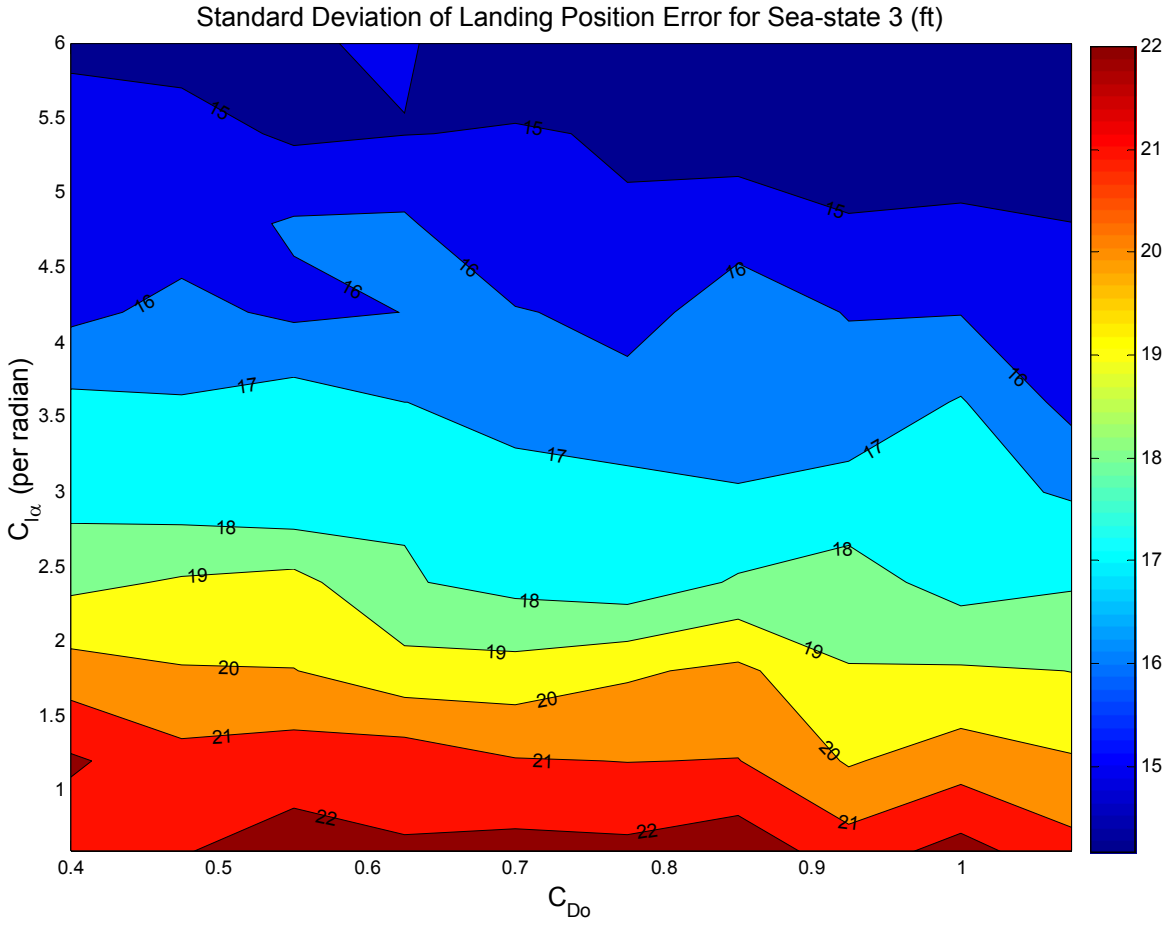

Figure 23: Sea-state 3 Landing Position Error Standard Deviation Contour

Figure 24 presents the RMS throttle control power for sea-state 3 with lift-curve slope increasing up the y-axis and drag increasing along the x-axis. Total drag contributed negligibly except at extremely low lift-curve slopes where increased drag resulted in less variation because of the higher drag for the trim condition.

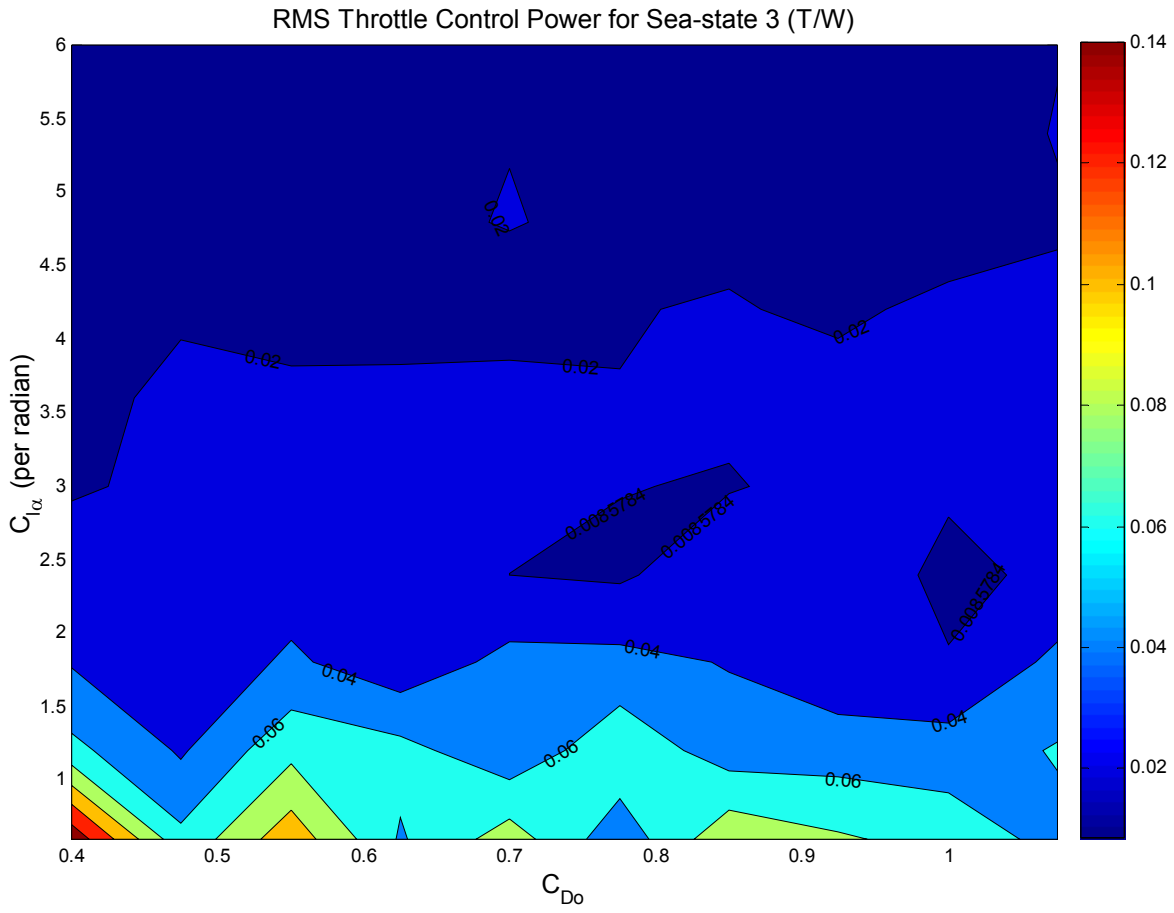

Figure 24: RMS Throttle Control Power for Sea-state 3

SUMMARY AND DESIGN IMPLICATIONS

The primary influence of gust intensity on minimum elevator power (demonstrated by Figures 19 and 20) and sea-state on throttle activity (demonstrated in Figures 21 and 24) was expected. The vertical flight path corrections required a change in the aircraft's energy. This is best accomplished by adjusting the throttle setting. The most significant gust effect is the vertical component disturbing the aircraft's pitch attitude. The elevator provides the compensating pitching moment.

The longitudinal stability had little influence on landing performance. This was expected because the stability determines the aircraft's open-loop response (response in the absence of control inputs) to disturbances. Because the automatic control system was continuously updating the control commands, the natural response played a negligible role in landing performance. Designing an aircraft to be unstable has approach speed and maximum landing weight benefits. The most unstable configurations presented in this section were the most desirable for every figure of merit evaluated. Within the scope of the tested range, this study does not indicate a limit on the amount of instability suitable for an autonomous carrier-based aircraft.

The drag coefficient had little effect on landing performance for the same reasons as longitudinal stability. For some manned aircraft, speedbrakes are deployed to allow approach to be flown on the front-side of the power curve where speed is stable rather than the back side of the power curve where speed is unstable. The automatic control system makes the small updates continuously. Consequently, the aircraft's natural stability is unimportant. This insensitivity to drag coefficient leaves a decision on speed brakes completely to the designer, and means that the landing dispersion would be robust to variations in drag, such as might be caused by combat damage or the carriage of external stores.

The lift curve slope was the dominant factor in all aspects of performance for the carrier-landing task; increasing the lift curve slope improved performance. This was the expected result because tracking the commanded altitude involved nothing more than shifting the airplane's flight path vertically about a trim condition, in our case a ramp representing the glide slope, perturbed by our diverse disturbances. A vertical shift in the flight path required a change in lift coefficient because the airspeed was tightly regulated as required. The lift curve slope represents the sensitivity of flight path angle change to change in AOA. The lift curve slope directly

determined the required change in AOA for the desired change in lift thereby determining all of the performance characteristics previously discussed. Future UCAV designs must carefully weigh the landing performance benefits of a high lift curve slope, with a minimum of 2.9 per radian, against other operational performance requirements. The minimum lift curve slope requirement constrains the minimum aspect ratio and the maximum wing sweep angle, the two primary geometric attributes of an aircraft.

CONCLUSIONS

Several specific conclusions were reached based on this simulation study. They are as follows:

a. Navigation errors, using the state-of-the-art satellite based systems, are small and result in negligible landing errors as demonstrated in Figure 13 and Table 6.

b. Gust intensity influences the required RMS elevator power, but results in negligible landing errors when modeled concurrently with any significant sea-state.

c. Ship motion is the dominant cause of landing errors. Landing dispersion and boarding rates are highly dependent on sea-state.

d. Longitudinal stability and drag coefficient has negligible influence on landing precision and control requirements. No limit on instability or range of acceptable drag coefficient was indicated.

e. Lift curve slope is the dominant aircraft attribute for all landing performance criteria and each improves with increasing lift curve slope. The minimum lift curve slope for suitable longitudinal landing performance is 2.9 per radian.

RECOMMENDATIONS

The effect of direct lift control (DLC) should be investigated. DLC acts in the direction of desired control, while throttle and elevator control altitude only indirectly. Also, because DLC is a small, light-weight control surface it is capable of very high bandwidth activity. DLC will likely reduce the strong dependency upon lift curve slope since it provides direct control over the flight path angle.

An investigation should be conducted to determine the performance of alternative control structures such as eigenstructure assignment or an LQR controller that incorporates the known ship accelerations in addition to the ship rates and position. The `lqry` gains used in this study automatically assigned high frequency control to the elevator and low frequency control to throttle, but this may not be the case when a third control input is introduced to the system.

An investigation should be conducted for lateral mode aircraft dynamics. This is a more complex problem because of the coupling of the airplane's lateral and directional axes, plus the coupling of the ship's lateral and directional axes.

BIBLIOGRAPHY

Clark, Vern. “Sea Power 21,” *Proceedings*. U.S. Naval Institute, October, 2002 (available from http://www.usni.org/Proceedings/articles02/proCNO10.htm).

Etkin, Bernard. *Dynamics of Flight*. John Wiley & Sons, 1959.

Heffley, Robert, *Outer-Loop Control Factors For Carrier Aircraft*. Report number: RHE-NAV-90-TR-1, Naval Air Systems Command, DEC 90.

Kaminer, I., A.M. Pascoal, P.P. Khargonekar, and E. Coleman, ``A Velocity Algorithm for the Implementation of Nonlinear Gain-Scheduled Controllers", *Automatica*, Vol. 31, pp. 1185--1191,1995.

McRuer, Ashkenas, and Graham. *Aircraft Dynamics and Automatic Control.* Princeton University Press, 1973.

Mulder, J.A. and Van der Vaart, J.C. "Lecture Notes Dictaat D-47: Aircraft Response to Atmospheric Turbulence", Delft University, 1993.

Nelson, Robert C. *Flight Stability and Automatic Control*. Second ed. McGraw-Hill, 1998.

Rudowsky *et al*. *Review of the Carrier Approach Criteria for Carrier-Based Aircraft Phase I; Final Report*. Report number: NAWCADPAX/TR-2002/71, Naval Air Systems Command, OCT 02.

Schug *et al*. "Guidance and Control for Shipboard Automatic Landing Using GPS," draft report.

U.S. Naval Test Pilot School Flight Test Manual No. 103, *Fixed Wing Stability and Control: Theory and Flight Test Techniques*. Patuxent River, 1997.

Waters *et al*., "Test Results of an F/A-18 Automatic Carrier Landing Using Shipboard Relative GPS," draft report.

Waters, Jack. Carrier Suitability Department Head, Naval Strike Aircraft Test Squadron. "Ship Landing Issues" PowerPoint Presentation.

APPENDIX I : LONGITUDINAL SIMULATION CODE (version 20.03.03)

```
% synthesis model and simulation script for Trident project
% inner-outer loop variant
clear all
configuration=('A-4, (trial,CLalp .6:.6:6, Cmalp-.65:.1:.25) Sea 3 ');

load Sea3        % Sea states 3,4,5 are available
                    % Shiptrans=[surge,sway,heavedn]; (ft)
ShipAngles=ship_out(:,1:3); (roll,pitch,yaw)

% These 3 lines determine the rates of pitch and heave. They're used later as
sensed signals in the controller.
% These signals could be generated by the ship motion model. They just need
to be re-run.
[nS,mS]=size(ShipAngles);
randn('state',sum(100*clock));      %insures random setting for rand function
rand('state',sum(100*clock));       %not sure if the above initiates both
random functions

delT=0.01;     %time step size for ship model and aircraft simulation
Sigma_nav=0.6467;                % ft
Vwind=20*1.69;       % fps
Glideslope=3.5*pi/180;
tGlide=tan(Glideslope);
d_init=6000;              % ft
h_init=d_init*tGlide;    % ft

ShipV=16.878;        %ship average velocity (fps)
ShipL=223;           % ft from C.M. aft to L.A.
ShipH=64;            % ft from C.M. up to L.A.
ShipW=-10;           % ft from C.M. right (starboard) to L.A.
ship=(Shiptrans(:,1)+ShipH*ShipAngles(:,2))*tGlide-ShipL*ShipAngles(:,2)-
Shiptrans(:,3); % positive up
shiprate=(ship(2:nS)-ship(1:nS-1))/delT;
   % 'ship' is the vertical movement of the landing area (positive up)...
   % four components: surge, fore-aft displacement due to pitch (these two
   % are multiplied by tGlide), vert displacement due to pitch, and
heave(positive down)


M=0.2;
a=1116;             % ft/s
p=2116;              % psf
ro=.00238;
u0=a*M;              % TAS fps
q=.5*ro*u0^2;        % psf
S=260;               % ft^2
c=10.8;               % ft
W=17578;             % lbs
mass=W/32.2;         % slugs
Iy=29930;             % slug-ft^2              %%%Gear down
Ix=16450;                % slug-ft^2
Iz=35220;            % slug-ft^2
Ixz=-5850;           % slug-ft^2
Theta0=0;            % flight path angle
```

```
g=32.2;              % fps

mm=ceil(1.2*d_init/(u0-Vwind-ShipV)/delT);

% Dryden Gust Model
% Gust variables and matrix construction

L_g=69;      %meters
sigma_wg=0.229 *Vwind;
sigma_ug=1.2*sigma_wg;

A_gust=[-u0/L_g 0 0; ...
        0 0 1;...
        0 -u0^2/L_g^2 -2*u0/L_g];
B_gust=[sigma_ug*sqrt(2*u0/L_g) 0;...
        0 sigma_wg*sqrt(3*u0/L_g);...
        0 (1-2*sqrt(3)*sigma_wg*sqrt((u0/L_g)^3))];
C_gust=eye(2,3);

% find discrete time gust system
Csys_gust=ss(A_gust,B_gust,C_gust,zeros(2));  %continuous system
Dsys_gust=c2d(Csys_gust,delT);                %Discrete


CLo=W/(q*S);
CDo=0.038*4+.2*CLo^2;   % k was estimated at 0.2  assuming e=0.55 the *4 is
for landing gear, flaps, and speed brake
CLalp=3.5;            %this, CDo, and Cmalp will be varied in a loop to
analyze influence on landings
CDalp=0.56;
Cmalp=-0.41;
CLalpdot=1.12;
Cmalpdot=-1.65;
CLq=0;
Cmq=-4.3;
CLM=0.15;       CLu=M*CLM;
CDM=0.03;        CDu=M*CDM;
CmM=-0.05;      Cmu=M*CmM;
CLe=0.4;
Cme=-0.6;
e_max=0.5;

%initialize variables for collecting landing statistics
x_error=zeros(1000,10,10);
h_std_error=zeros(1000,10,10);
Vclosure=zeros(1000,10,10);
Theta_std=zeros(1000,10,10);
AOA_std=zeros(1000,10,10);
Hclose=zeros(1000,10,10);
speed=zeros(1000,10,10);
aspeed=zeros(1000,10,10);
AOAave=zeros(1000,10,10);
controls=zeros(mm,2,10,10);


Cm_count=0;
```

```
% start loop #1: variation on C_m_alpha

for Cmalp=-.65:.1:.25         %for Cmalp=-.65:.1:.25
    Cm_count=Cm_count+1;

% start loop #2: variation on C_L_alpha

for slope=0.6:0.6:6  %slope is limited to less than 2*pi, theoretical limit

   CLalp=slope;

% calculate long stab dimensional stability derivatives:

Xu=-(CDu+2*CDo)*q*S/mass/u0;
Xw=-(CDalp-CLo)*q*S/mass/u0;
Xt=0;
Xe=0;
XeT=g;                                % Thrust measure in percent T/W

Zu=-(CLu+2*CLo)*q*S/mass/u0;
Zw=-(CLalp+CDo)*q*S/mass/u0;
Zwdot=-CLalpdot*c*q*S/2/u0^2/mass;     % this is suspected in error
Ze=-CLe*q*S/mass;
ZeT=0;

Mu=Cmu*q*S*c/u0/Iy;
Mw=Cmalp*q*S*c/u0/Iy;
Mwdot=Cmalpdot*q*S*c^2/u0^2/2/Iy;
Mq= Cmq*c*q*S*c/2/u0/Iy;
Me=Cme*q*S*c/Iy;
MeT=0;

%%%%%% build the synthesis model

% states- u, w, q, theta, h, h/s, u/s
A=zeros(7);
A(1,1:6) = [Xu, Xw, 0, -g, 0, 0];                                  % du
A(2,1:6) = [Zu, Zw, u0, 0, 0, 0];                                   % dalpha
A(3,1:6) = [Mu+Mwdot*Zu, Mw+Mwdot*Zw, Mq+Mwdot*u0, 0, 0, 0];   % dq
A(4,1:6) = [0 0 1 0 0 0];                                          % dtheta
A(5,1:6) = [0 -1 0 u0 0 0];                                        % dh
A(6,1:6)= [0 0 0 0 1 0];                                           % h
A(7,:)=[1 0 0 0 0 0 0];                                          % u

% gust inputs {horizontal/ vertical (fps)}
B1=zeros(5,2);
B1(1:3,1:2)=[Xu,Xw; Zu,Zw; Mu,Mw];

% controlled inputs (u2) : elevator (rad), thrust (%T/W)
B2=[Xe, XeT;
   Ze, ZeT;
   Me+Mwdot*Ze, MeT+Mwdot*ZeT;
   zeros(4,2)];

% Design an controller for the throttle using LQR
Cs=[1 0 0 0 0 0 0.5;0 -1 0 u0 3 3 0];
Ds=zeros(2,2);
```

```
% output weights for sfb gains
Su=3.5*1.69;                        %fps- defined by 7 kt variability
Sh=1;
Se=10*pi/180;
ST=0.1;

% Calculate sfb gains for synthesis plant using output weighted LQR

Q=diag([1/Su, 1/Sh]);
R=diag([1/Se 1/ST]);
syn_model=ss(A,B2,Cs,Ds);
dsyn_model=c2d(syn_model,delT);

[K,SRic,E]=lqry(dsyn_model,Q,R);

% find the discrete realization for simulation
[Ad,Bd,Cd,Dd]=ssdata(dsyn_model);             % Unpacked Discrete System

% SIMULATION
% start loop #3: Monte-Carlo

for trial=1:1000,

% Initialize simulation run
i=1;

X=zeros(5,mm);                                % Stores the states
X(5,1)=h_init;                                 % initialize the states

h_cmd=zeros(1,mm);
h_cmd(1)=h_init;
u=zeros(2,mm);
h_error=zeros(1,mm);
h_error_rate=zeros(1,mm);
u_integ=[0;0];
x=zeros(1,mm);
x(1)=d_init;

% JPALS altitude error
nav=Sigma_nav*randn(mm,1);
%nav=zeros(mm,1);    %activate this line to turn nav errors off

Gust=lsim(Dsys_gust,randn(mm,2),[]);
%Gust=zeros(mm,2);   %activate this line to turn gusts off


% Build disturbance inputs
% leave the pitch rate, theta, integrator noise zero

% this is where a routine is needed to randomize the start conditions
Shiptime=round(rand(1)*45000)+1; %random to simulate all ship motion phase
relationships
Disturbance([1 2 5 7 8],:)=[Gust,nav,ShipAngles(Shiptime:mm+Shiptime-
1,2),Shiptrans(Shiptime:mm+Shiptime-1,3)]';
```

```
% start loop #4: time step simulation

while X(5,i) >=(13.62-(x(i)+Shiptrans(i+Shiptime-1,1)-
ShipH*Disturbance(7,i))*Disturbance(7,i)-Disturbance(8,i)),    % accounts for
ship pitch, surge, and heave

   i=i+1;
   if i==mm
      % safety condition to prevent falling into infinite loop
      warning('i=mm  flying slow')
      x(i)
      avespeed=sum(X(1,:))/i
      break
   end

    % calculate the lateral distance from the origin (integrate velocity)
    x(i)=x(i-1)-(u0-ShipV-Vwind+X(1,i-1))*delT;       % u0-ShipV-Vwind+X(1,i-
1)=closing velocity

    % h_cmd is the sum of the glideslope, and its time varying ship motion
    h_cmd(i)=x(i)*tGlide+ship(i+Shiptime-1);

    % simulation step (5 more integrations here)
    %      dynamics              control inputs      2-dim gust
    X(:,i)=Ad(1:5,1:5)*X(:,i-1)+ Bd(1:5,:)*u(:,i-1)+
delT*B1(:,1:2)*Disturbance(1:2,i);

    % calculate true altitude error
    h_error(i)=X(5,i)-h_cmd(i);
    % calculate altitude error rate
    %               acft sink rate      ship rate   glideslope bias
    h_error_rate(i)=A(5,1:4)*X(1:4,i)-(shiprate(i+Shiptime-1)-(u0-ShipV-
Vwind+X(1,i-1))*tGlide);

   % integral action within the controller
   u_integ= u_integ + delT*K(:,5:7)*[h_error_rate(i);
   h_error(i)+nav(i);X(1,i)];

   % calculate elevator and throttle command for next time step
   u(:,i)= -K(:,1:4)*X(1:4,i) - u_integ;

end % loop #4

% collect statistic for simulation run

bb=round(i/8);  % start here to chop off start-up errors
X=X(:,bb:i); h_cmd=h_cmd(bb:i);
hdot=A(5,1:4)*X(1:4,:);
x=x(bb:i);
u=u(:,bb:i);
h_error=h_error(:,bb:i);
Disturbance=Disturbance(:,bb:i);
Gust=Gust(bb:i,:);
L=length(h_error);
count_sl=round(slope/.6);
z1=X(5,L-1)-(13.62-(x(L-1)-ShipH*Disturbance(7,L-1))*Disturbance(7,L-1)-
Disturbance(8,L-1));
```

```
z2=X(5,L)-(13.62-(x(L)-ShipH*Disturbance(7,L))*Disturbance(7,L)-
Disturbance(8,L));
xland=(x(L-1)-x(L))*z1/(z1-z2)+x(L-1);
x_error(trial,count_sl,Cm_count)=ShipL-xland;          %positive error means
landing was long

% error stats  [h_error @LA, average
h_error,theta_perterbation,aoa_perterbation,vert closure, h_dot,x_dot]
h_std_error(trial,count_sl,Cm_count)= std(h_error);      %standard deviation
of altitude error during flight
% vertical rate ignores: true landing distance (this would be easy to adopt),
% and heave rate (negligible)
Vclosure(trial,count_sl,Cm_count)=shiprate(i+Shiptime-1)-hdot(L);
Hclose(trial,count_sl,Cm_count)=X(1,L)+u0-ShipV-Vwind;
aspeed(trial,count_sl,Cm_count)=sum(X(1,:))/L;
Theta_std(trial,count_sl,Cm_count)=std(X(4,:)-sum(X(4,:)/L));
AOA_std(trial,count_sl,Cm_count)=std(X(2,:))/(u0+aspeed(trial,count_sl,Cm_cou
nt));
AOAave(trial,count_sl,Cm_count)=sum(X(2,:)/L)/(u0+aspeed(trial,count_sl,Cm_co
unt));
speed(trial,count_sl,Cm_count)=std(X(1,:));
Disturbance=zeros(8,mm);


end   %end trial loop (loop #3)
controls(1:L,:,count_sl,Cm_count)=u';
controls(mm,:,count_sl,Cm_count)=L;


save Lnd_StatN12 x_error h_std_error Vclosure Hclose Theta_std AOA_std
configuration speed aspeed AOAave controls

end      % end loop changing Clalp (loop #2)
Cm_count

end      %end loop for Cmalp (loop #1)
```

APPENDIX II : PLAN OF ACTION AND MILESTONES

Due	Status	Task	Action
19-Aug		**Fall Semester Classes Begin**	
	done	JPALS signal analysis for frequency content	Sweger
	done	Basic longitudinal glide slope tracking model	Sweger
2-Sep		**Holiday -- Labor Day**	
	done	Define ship motion influences on the landing area	Sweger
13 -15 Sept		**1/C Parents Weekend**	
	done	Write a section on the ship motion and equations	Sweger
	done	Write a section on JPALS model	Sweger
14-Oct		**Holiday -- Columbus Day**	
	done	Integrate ship motion into flight model	Sweger
	done	Build gust model	Sweger
	done	Integrate gust model	Sweger
	done	Write section on gust model	Sweger
11-Nov		**Holiday -- Veteran's Day**	
	done	Define synthesis model for H-infinity controller	Sweger/Niewoehner
	done	Write section on manned vs. unmanned issues	Sweger
		Debug H-infinity controller	Niewoehner
	done	Write section on the over all model	Sweger
28-Nov		**Holiday -- Thanksgiving**	
	done	Compile sections for interim report	Sweger
		Revise interim report	Sweger
4-Dec		**NLT NOON: Submit, via e-mail, POA&M to Dean Miller ("cc" adviser and DDRS)**	
4-Dec		**NLT 1400: Submission of Interim Trident Scholar Reports to DDRS**	

		Begin building lateral mode simulation model	Sweger
6-Dec		**End of Fall Semester Classes**	
		Build a data collection structure for the sensitivity analysis	Sweger
		Begin sensitivity analysis on longitudinal mode	Sweger
10-Dec - 3-Jan		**End of Semester Leave**	
Due	**Status**	**Task**	**Action**
7-Jan		**Spring Semester Classes Begin**	
		Continue attempts to incorporate lead compensation	Hallberg/Niewoehner
20-Jan		**Holiday -- Martin Luther King Day**	
		Control structure fixed	Hallberg/Niewoehner
17-Feb		**Holiday -- President's Day**	
		Run simulations for sensitivity analysis	Sweger
		Restrict study to longitudinal characteristics only due to	
		time constraints	
7-Mar - 16-Mar		**SPRING BREAK**	
		Compile longitudinal simulation results from sensitivity analysis	Sweger
		Anaylze the sensitivity to lift curve slope and elevator power	Sweger
		Anaylze the sensitivity to throttle lag and moment of inertia	Sweger
		Anaylze sensitivity to sea-state and wind-over-deck	Sweger
		Begin preparing final presentation	Sweger
		Prepare results graphics for report	Sweger
		Run simulations to fill gaps discovered during the writing phase	Sweger
		Write draft criteria	Sweger
		Continue working on final report	Sweger
		Proof read report	Niewoehner
		Revise presentation, practice presenting	Sweger
18-Apr		**Submission of "Cmte-Ready" Versions of Trident Scholar Reports to DDRS**	
24-Apr		**Day 1: Trident Scholar Conference**	
25-Apr		**Day 2: Trident Scholar Conference**	

26-Apr		**Trident Scholar Poster Session and Banquet**	
29-Apr		**End of Spring Semester Classes**	
		Finish revising final report	Sweger
5-May		**Submission of Final Versions of Trident Scholar Reports to DDRS**	
23-May		**Graduation Class of 2003**	

APPENDIX III : SHIP MOTION SIMULATION CODE

```
% ************************************************************************
% CVN65dynamics  CVN 65 motion constants generated from SMP program, NSRDC
%                (David Taylor). Ship speed = 15 knots, 30 deg relative to
%                long crested waves, wave period = 15 sec.
%
%        Sea State           Wave Height
%            3                  8.2 ft
%            4                  13.1 ft
%            5                  19.7 ft.
%
% Raw amplitudes correspond to 2*RMS but are scaled for 3*RMS using "kmot".
% Therefore, maximum amplitudes of motion are simulated.
%
% ************************************************************************
% $Header:
\\\\Uavlabnt1\\UAVLab\040Share\\Projects\\CVS_ROOT/F18_JPALS/F18Sim/CVN65dyna
mics.m,v 1.3 2001/01/05 17:06:13 AksteterJW Exp $
% ************************************************************************
% Changes:
%
% $Log: CVN65dynamics.m,v $
% Revision 1.3  2001/01/05 17:06:13  AksteterJW
% Slight documentation mod. for clarification.  Also,
% some spec. disturbance frequencies under each sea state were equivalent.
% So some frequencies were adjusted rel. to their spec. values so that they
% differ by >= 0.05 rad/sec relative to one another.  This gives dissimilar
% beat frequencies, hence more statistically meaningful simulations.  The
% spec. values were added in parentheses to the right for reference.
%
% Revision 1.2  2000/12/05 19:17:41  AksteterJW
% Documentation including input and output parameter definitions.
%
%
% ************************************************************************
%                            Inputs
%************************************************************************
% iseastate    Sea state value (e.g., 3, 4, or 5)
% iship        Switch for oscillatory ship motion
(sway,heave,etc.)[0=off;1=on]
%
%************************************************************************
%                            Outputs
%************************************************************************
%  surgeamp    Amplitude of ships surge motion (ft)
%  surgefreq   Frequency of ships surge motion (rad/sec)
%  yawamp      Amplitude of ships yaw motion (deg)
%  yawfreq     Frequency of ships yaw motion (rad/sec)
%  swayamp     Amplitude of ships sway motion (ft)
%  swayfreq    Frequency of ships sway motion (rad/sec)
%  heaveamp    Amplitude of ships heave motion (ft)
%  heavefreq   Frequency of ships heave motion (rad/sec)
%  pitchamp    Amplitude of ships pitch motion (deg)
%  pitchfreq   Frequency of ships pitch motion (rad/sec)
%  rollamp     Amplitude of ships roll motion (deg)
```

```
%  rollfreq    Frequency of ships roll motion (rad/sec)
%**************************************************************************

if iseastate==3                                          % if iseastate==3
% ************************************************************************
%                        SHIP MOTION CONSTANTS (3*RMS)
%                            CVN 65 Sea State 3
% ************************************************************************
kmot=1.5;                                                %Motion Scaling
iiship=kmot*iship;

%  The following ship motions are driven by sine waves
 surgeamp     = 0.8*iiship;  % Amplitude of ships surge motion (ft)
 surgefreq    = 0.35;        % (0.45) Frequency of ships surge motion
(rad/sec)

 yawamp       = 0.12*iiship; % Amplitude of ships yaw motion (deg)
 yawfreq      = 0.63;        % (0.63) Frequency of ships yaw motion (rad/sec)

 swayamp      = 0.53*iiship; % Amplitude of ships sway motion (ft)
 swayfreq     = 0.45;        % (0.45) Frequency of ships sway motion
(rad/sec)

 heaveamp     = 1.99*iiship; % Amplitude of ships heave motion (ft)
 heavefreq    = 0.53;        % (0.48) Frequency of ships heave motion
(rad/sec)

 pitchamp     = 0.72*iiship; % Amplitude of ships pitch motion (deg)
 pitchfreq    = 0.58;        % (0.57) Frequency of ships pitch motion
(rad/sec)

 rollamp      = 0.21*iiship; % Amplitude of ships roll motion (deg)
 rollfreq     = 0.40;        % (0.57) Frequency of ships roll motion
(rad/sec)

elseif iseastate==4
% ************************************************************************
%                        SHIP MOTION CONSTANTS (3*RMS)
%                            CVN 65 Sea State 4
% ************************************************************************
kmot=1.5;                                              %Motion Scaling
iiship=kmot*iship;

%  The following ship motions are driven by sine waves
 surgeamp     = 1.32*iiship; % Amplitude of ships surge motion (ft)
 surgefreq    = 0.35;        % (0.45) Frequency of ships surge motion
(rad/sec)

 yawamp       = 0.30*iiship; % Amplitude of ships yaw motion (deg)
 yawfreq      = 0.50;        % (0.52) Frequency of ships yaw motion (rad/sec)

 swayamp      = 0.84*iiship; % Amplitude of ships sway motion (ft)
 swayfreq     = 0.40;        % (0.45) Frequency of ships sway motion
(rad/sec)

 heaveamp     = 3.59*iiship; % Amplitude of ships heave motion (ft)
```

```
 heavefreq     = 0.55;         % (0.48) Frequency of ships heave motion
(rad/sec)

 pitchamp      = 1.15*iiship; % Amplitude of ships pitch motion (deg)
 pitchfreq     = 0.60;         % (0.57) Frequency of ships pitch motion
(rad/sec)

 rollamp       = 0.33*iiship; % Amplitude of ships roll motion (deg)
 rollfreq      = 0.45;         % (0.45) Frequency of ships roll motion
(rad/sec)

elseif iseastate==5
% ********************************************************************
%                       SHIP MOTION CONSTANTS (3*RMS)
%                           CVN 65 Sea State 5
% ********************************************************************
kmot=1.5;                                                %Motion Scaling
iiship=kmot*iship;

%  The following ship motions are driven by sine waves
 surgeamp      = 1.98*iiship; % Amplitude of ships surge motion (ft)
 surgefreq     = 0.32;         % (0.45) Frequency of ships surge motion
(rad/sec)

 yawamp        = 0.29*iiship; % Amplitude of ships yaw motion (deg)
 yawfreq       = 0.52;         % (0.52) Frequency of ships yaw motion (rad/sec)

 swayamp       = 1.26*iiship; % Amplitude of ships sway motion (ft)
 swayfreq      = 0.37;         % (0.45) Frequency of ships sway motion
(rad/sec)

 heaveamp      = 4.77*iiship; % Amplitude of ships heave motion (ft)
 heavefreq     = 0.42;         % (0.48) Frequency of ships heave motion
(rad/sec)

 pitchamp      = 1.73*iiship; % Amplitude of ships pitch motion (deg)
 pitchfreq     = 0.57;         % (0.57) Frequency of ships pitch motion
(rad/sec)

 rollamp       = 0.49*iiship; % Amplitude of ships roll motion (deg)
 rollfreq      = 0.47;         % (0.45) Frequency of ships roll motion
(rad/sec)

else
% ********************************************************************
%                       SHIP MOTION CONSTANTS (3*RMS)
%                            sea state 0
% ********************************************************************
kmot=1;                 %Motion Scaling
iiship=kmot*iship;

%  The following ship motions are driven by sine waves
 surgeamp      = 0*iiship;    % Amplitude of ships surge motion (ft)
 surgefreq     = 0;           % Frequency of ships surge motion (rad/sec)

 yawamp        = 0*iiship;    % Amplitude of ships yaw motion (deg)
 yawfreq       = 0;           % Frequency of ships yaw motion (rad/sec)
```

```
 swayamp      = 0*iiship;    % Amplitude of ships sway motion (ft)
 swayfreq     = 0;           % Frequency of ships sway motion (rad/sec)

 heaveamp     = 0*iiship;    % Amplitude of ships heave motion (ft)   6.0
 heavefreq    = 0;           % Frequency of ships heave motion (rad/sec)

 pitchamp     = 0*iiship;    % Amplitude of ships pitch motion (deg)  1.6
 pitchfreq    = 0;           % Frequency of ships pitch motion (rad/sec)

 rollamp      = 0*iiship;    % Amplitude of ships roll motion (deg)
 rollfreq     = 0;           % Frequency of ships roll motion (rad/sec)

end                                                % END if iseastate==3


function IJK=geod2ecef(lat,lon,alt)
% function IJK=geod2ecef(lat,lon,alt)
% Convert Earth Centered Earth Fixed (ECEF) Cartesian coordinates
% to Geodetic coordinates
% inputs:
%   lat  - Geodetic Latitude (deg)
%   lon  - Geodetic Longitude (deg)
%   alt  - Geodetic Altitude (ft);
% outputs:
%   x   Equatorial Prime meridian coordinate (ft)
%   y   Equatoral 90 deg Long. coordinate (ft)
%   z   North coordinate (ft)
% uses WGS-84 Ellipsoidal Model.
%
%%%%%%%%%%%%%%%%%%%%%%%%%%%%%%%%%%%%%%%%%%%%%%%%%%%%%%%%%%%%
% 6/14/99
%  Eric Schug (SAIC)
%%%%%%%%%%%%%%%%%%%%%%%%%%%%%%%%%%%%%%%%%%%%%%%%%%%%%%%%%%%%
% $Header:
\\\\Uavlabnt1\\UAVLab\040Share\\Projects\\CVS_ROOT/F18_JPALS/F18Sim/geod2ecef
.m,v 1.2 2002/05/29 15:15:11 SchugEC Exp $

% Changes
% $Log: geod2ecef.m,v $
% Revision 1.2  2002/05/29 15:15:11  SchugEC
% Restoring Lastest F18_JPALS after deleting CVS files
%
% Revision 1.3  2002/03/22 21:47:39  SchugEC
% vectorized it
%
% Revision 1.2  2001/12/12 20:46:27  AksteterJW
% Header documentation.
%
% Revision 1.1  2000/10/26 18:39:53  SchugEC
% Initial addtions
%
%%%%%%%%%%%%%%%%%%%%%%%%%%%%%%%%%%%%%%%%%%%%%%%%%%%%%%%%%%%%


%%%%%%%%%%%%%%%%%%%%%%%%%%%%%%%%%%%%%%%%%%%%%%%%%%%%%%%%%%%%
```

```
% Constants Originally in MKS units, converted to ft,sec
%%%%%%%%%%%%%%%%%%%%%%%%%%%%%%%%%%%%%%%%%%%%%%%%%%%%%%%%
m2ft = 3.28083989501312;
a = 6378137.0*m2ft;             % semi-major axis
e2 = 6.69437999014e-3;          % First Eccentricity Squared
ELIN = 5.2185400842339e5*m2ft; % Linear Eccentricity
E2 =  ELIN*ELIN;
b_a=0.996647189335; % major/minor axis ratio

lat=lat*pi/180;
lon=lon*pi/180;
fslat=sqrt(1-e2*sin(lat).^2);
Rp=a./fslat;
IJK(:,1)=(Rp+alt).*cos(lat).*cos(lon);
IJK(:,2)=(Rp+alt).*cos(lat).*sin(lon);
IJK(:,3)=(Rp.*b_a.^2+alt).*sin(lat);


% load_ship

kts2fps = 1.6878;
fps2kts = 1/kts2fps;

%*********************************************
% You can adjust these
ShipCMlat = 0;
ShipCMlon = 0;
iseastate = 3;
tend = 10;
spi = 10*kts2fps;    % ship speed in ft/sec
turntime = 5;  % time when ship turn starts (sec)
turndeg = 0;   % desired ship turn angle (deg)
psiski = 0;    % initial ship heading (deg)
%*********************************************

ishpmotion = 'CVN65';
iship = 1;   % 1=ON, 0=OFF
dt = 0.01;
nsave = 1;
numpts = inf;
d2r = pi/180;

fprintf('Ship CM Latitude  = %7.2f (deg) \n',ShipCMlat)
fprintf('Ship CM Longitude = %7.2f (deg) \n',ShipCMlon)
fprintf('Ship Motion: %-9.9s Sea State %2d \n', ishpmotion,iseastate)
fprintf('Simulation run time = %7.2f (sec) \n',tend)
fprintf('Ship Velocity         =%8.2f kts\n',spi*fps2kts)

ShipCMecef=geod2ecef(ShipCMlat,ShipCMlon,0);

CVN65dynamics

seedsize = max(1,1);
rand('seed',999)
delphase=2*pi*rand(6,seedsize); % repeatable phase set for ionce =
1==>maxautorun
```

```
   surgephase = delphase(1,1);   % Initial phase of surge motion (rad)
   yawphase   = delphase(2,1);   % Initial phase of yaw motion (rad)
   swayphase  = delphase(3,1);   % Initial phase of sway motion (rad)
   heavephase = delphase(4,1);   % Initial phase of heave motion (rad)
   pitchphase = delphase(5,1);   % Initial phase of pitch motion (rad)
   rollphase  = delphase(6,1);   % Initial phase of roll motion (rad)

% ********************************************************
%            Initial ship Euler rates (local frame)
% ********************************************************
psid_0=(yawamp*yawfreq*cos(yawphase))*d2r;        % Heading rate, rad/s
(+cwn)
thed_0=(pitchamp*pitchfreq*cos(pitchphase))*d2r;  % Pitch rate, rad/s (+bow
up)
phid_0=(rollamp*rollfreq*cos(rollphase))*d2r;     % Roll rate, rad/s (+stbd
dn)

   %
************************************************************************
   %                      Call the SIMULINK simulation
   %
************************************************************************
   %  Simulation Setup
   tol = 1e-4;
   minstep = dt;
   maxstep = dt;
   tfinal = tend;

   simstruct=simset('Solver','ode1','FixedStep',dt,'OutputVariables','t',...
                    'Decimation',nsave,'RelTol',tol);
   [time]=sim('ship',tfinal,simstruct);
```